Lahar events in the last 2,000 years from Vesuvius eruptions. Part 1: Distribution and impact on densely inhabited territory estimated from field data analysis

Mauro A. Di Vito (1*), Ilaria Rucco (2), Sandro de Vita (1), Domenico M. Doronzo (1), Marina Bisson (3), Mattia de' Michieli Vitturi (3), Mauro Rosi (4), Laura Sandri (5), Giovanni Zanchetta (4), Elena Zanella (6), Antonio Costa (5)

(1) Istituto Nazionale di Geofisica e Vulcanologia - Sezione di Napoli Osservatorio Vesuviano, Napoli, Italy

(2) Heriot-Watt University, School of Engineering and Physical Sciences, Edinburgh, United Kingdom

(3) Istituto Nazionale di Geofisica e Vulcanologia - Sezione di Pisa, Pisa Italy

(4) Università di Pisa, Dipartimento di Scienze della Terra, Pisa, Italy

(5) Istituto Nazionale di Geofisica e Vulcanologia - Sezione di Bologna, Bologna, Italy

(6) Università di Torino, Dipartimento di Scienze della Terra, Torino, Italy

*Corresponding author: Mauro A. Di Vito (mauro.divito@ingv.it)

Abstract

Lahars represent some of the most dangerous phenomena in volcanic areas for their destructive power, causing dramatic changes in the landscape with no premonitory signs and impacting on population and infrastructures. In this regard, the Campanian Plain turns out to be very prone to the development of these phenomena, since the slopes of the Somma-Vesuvius and Campi Flegrei volcanoes, along with the Apennine reliefs are mantled by pyroclastic deposits that can be easily remobilized, especially after intense and/or prolonged rainfall.

This study focuses on the analysis of the pyroclastic fall and flow deposits and of the syn- and post-eruptive lahar deposits related to two sub-Plinian eruptions of Vesuvius, 472 CE (Pollena) and 1631. To begin with, historical and field data from the existing literature and from hundreds of outcrops were collected and organized into a database, which was integrated with several new pieces of data. In particular, stratigraphic, sedimentological (facies analysis and laboratory) and archaeological analyses were carried out, in addition to rock magnetic investigations and impact parameter calculations. The new data are also referred to the finding of ash beds in more distal areas, which were included into new isopach maps for the two sub-Plinian eruptions.

The results show that for both the eruptions the distribution of the primary deposits is wider than previously known. A consequence of these results is that a wider areal impact should be expected in terms of civil protection, as the sub-Plinian scenario is the reference one for a future large eruption of Vesuvius. Such distribution of the pyroclastic deposits directly affects the one of the lahar deposits, also because a significant remobilization took place during and after the studied eruptions, which involved the distal phreatomagmatic ash. From these integrated analyses, it was possible to constrain the timing of the deposition and the kind of deposits remobilized (pyroclastic fall vs. flow), as well as was possible to calculate the velocities and dynamic pressures of the lahars, and ultimately infer the lahar transport and emplacement mechanisms.

The multidisciplinary approach adopted in this work shows how it is crucial to assess the impact of lahars in densely populated areas even at distances of several to tens of km from active volcanoes. This especially applies to large parts of the densely populated areas around Somma-Vesuvius up to the nearby Apennine valleys.

Keywords: Somma-Vesuvius; Apennine valleys; pyroclastic deposits; lahars; areal distribution; local impact.

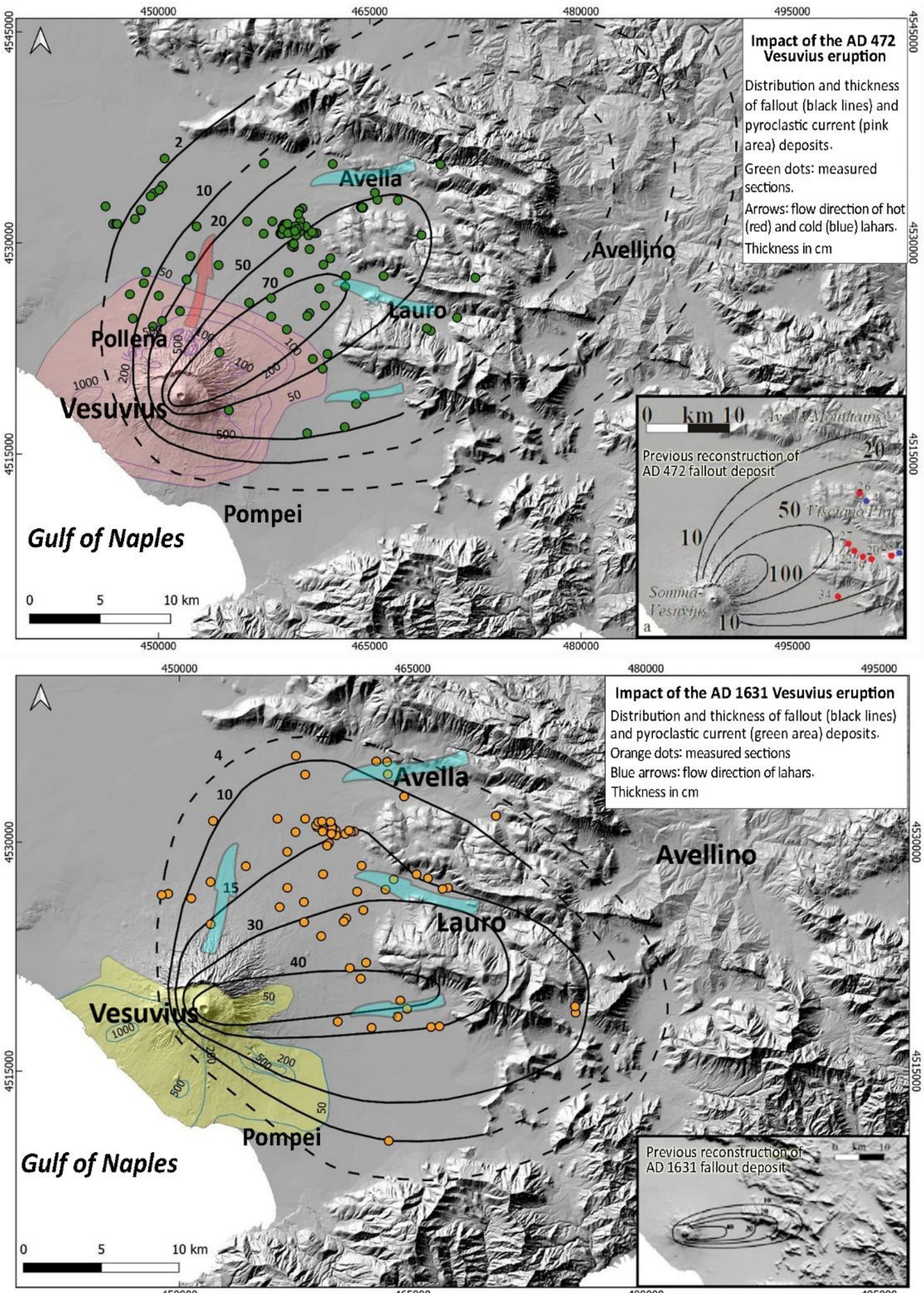
Impact of the AD 472 Vesuvius eruption
Distribution and thickness of fallout (black lines) and pyroclastic current (pink area) deposits.
Green dots: measured sections.
Arrows: flow direction of hot (red) and cold (blue) lahars.
Thickness in cm
Avella
Avellino
Lauro
Pollena
Vesuvius
Pompei
Gulf of Naples
Previous reconstruction of AD 472 fallout deposit
Impact of the AD 1631 Vesuvius eruption
Distribution and thickness of fallout (black lines) and pyroclastic current (green area) deposits.
Orange dots: measured sections
Blue arrows: flow direction of lahars.
Thickness in cm
Previous reconstruction of AD 1631 fallout deposit
0 5 10 km

Key figure

1. Introduction

The movement of volcaniclastic mass flows, and the consequent damage along the flanks of active volcanoes and perivolcanic plains, represent a constant threat to inhabited areas and populations (e.g., Waitt et al., 1983; Lowe et al., 1986; Pierson, 1985; Newhall and Punongbayan, 1996). Such systems are variably-fluidized, gravity-driven flows that consist of a mixture of pyroclastic sediment and water. They can be triggered by various mechanisms, among which the most common are intense or prolonged atmospheric precipitations (Arguden and Rodolfo, 1990; Rodolfo and Arguden, 1991; Pareschi et al., 2000; Rodolfo, 2000; Scott et al., 2001; Vallance and Iverson, 2015). Such precipitations or water runoff, especially during and/or after the eruptions, can cause the remobilization of pyroclastic deposits evolving into water-saturated multiphase systems called lahars (e.g., White et al., 1997; Sheridan et al., 1999; Scott et al., 2001; Baumann et al., 2020). The last century was affected by a significant number of highly-impacting lahar events associated to well-studied explosive volcanic eruptions worldwide, such as for example at Colima (Mexico) in 1913 (Rodriguez-Sedano et al., 2022), Nevado del Ruiz (Colombia) in 1985 (Voight, 1990), Ruapehu (New Zealand) in 2007 (Lube et al., 2012), and Merapi (Indonesia) in 2011 (Jenkins et al., 2015).

According to Rodolfo (2000), Sulpizio et al. (2006), and Vallance and Iverson (2015), volcaniclastic mass flows can be generated at variably-long time intervals, spanning from eruptive to post-eruptive phases of tens to hundreds of years. In case these flows are directly related to volcanic eruptions, that is occurring during or shortly after the eruptive event, lahars are defined as syn-eruptive, and can represent an important multihazard factor in the short-to-middle term for perivolcanic areas (Rodolfo, 2000; Sulpizio et al., 2006). Instead, in case they are unrelated to any eruption dynamics, that is occurring during long periods of volcanic quiescence, they are defined as post-eruptive (Vallance and Iverson, 2015), and can represent a long-term hazard factor (e.g., Siebe et al., 1999; Pareschi et al., 2002; Zanchetta et al., 2004a, 2004b; Sulpizio et al., 2006). Usually, post-eruptive lahars are not accounted for the assessment of volcanic hazard, although their study is important for hydrogeological hazard assessment and long-term territorial planning.

In this sense, that is from the hazard assessment point of view, one of the priorities concerns the assessment of those areas potentially exposed to such a threat, taking into account the temporal recurrences of the phenomena (over days to months after an eruption, or years to decades after) and physical features of the volcaniclastic mass flows (volume, thickness, velocity, dynamic pressure, concentration, and invasion areas). We stress the fact that the definition of syn-eruptive lahars (Sulpizio et al., 2006; Vallance and Iverson, 2015) adopted in the present work is important when accounting for the multihazard of explosive eruptions, which in areas like Vesuvius and surroundings should not be neglected for its assessment and mapping purposes (de'Michieli Vitturi et al., this issue; Sandri et al., this issue). The methodology used in this work is geological (see Section 3.2), and the syn-eruptive definition of lahars is necessary to avoid underestimations of the volcanic hazard from sub-Plinian eruptions at Vesuvius.

A lot of the existing literature analyzed the hazard related with volcaniclastic mass flows on the flanks of active volcanoes, through the reconstruction of historical and prehistoric events (e.g., Scott, 1989; Scott et al., 1995; Vallance and Scott, 1997; Zaragoza et al., 2020), by using empirical relationships or physical models (e.g., Macedonio and Pareschi, 1992; Costa, 1997; Iverson et al., 2000; Walsh et al., 2020). However, the areas affected by these phenomena can be extended well beyond the boundaries of the volcanic complex, also including the surrounding plains and the downwind-lying mountainous areas, which are subjected to tephra fallout sometimes even at great distances from the volcano (e.g., Siebe et al., 1999; Pareschi et al., 2000, 2002; Zanchetta et al., 2004a, 2004b; Di Crescenzo and Santo, 2005). In these areas, volcaniclastic mass flows may cause victims and damages, even where considered safe or scarcely affected by other volcanic hazards.

In this paper, we present the results of a multidisciplinary study, including geomorphological, stratigraphic, sedimentological and rock magnetic investigations, as well as impact parameter calculations by reverse engineering from the deposits. These investigations followed several surveying campaigns carried out in natural exposures, archaeological excavations, and trenches dug specifically for this purpose in the plain surrounding the Vesuvius edifice and along the Apennine valleys (Fig. 1). One of the goals of this study is to show the presence of lahar deposits even in areas several km far from the source areas of the Apennine hills and Somma-Vesuvius edifice, demonstrating the high mobility of these flows. Indeed, these two areas acted as source areas because they were largely affected by deposition of primary pyroclastic deposits from Plinian and sub-Plinian Somma-Vesuvius eruptions. The study of the past lahar deposits has been useful for the understanding of the feeding drainage basins, their extent and facies variations with distance from the source area, and the associated impact on landscape. As already pointed out by Di Vito et al. (2013, 2019), in the past 4.5 ka repeated lahar and flooding episodes related to the main eruptions of Somma-Vesuvius and Campi Flegrei volcanoes strongly stroke the Campanian Plain and its human settlements, influencing their partial or total abandonment. In particular, for the areas around Vesuvius, these phenomena included: i) large volume and high energy lahars, originated from the volcanic edifice, which affected the volcanic apron; ii) large flooding phenomena, i.e. overflowing of water affecting the Campanian plain; iii) lahars originated from the perivolcanic mountains that affected the Apennine valleys, and invaded the areas of the plain at their mouths. All of these phenomena differed to each other in terms of amount and grain-size of the involved sediment. The data and pieces of information described here were the basis for validating a new model for lahar transport (de' Michieli Vitturi et al., this issue), which was applied for assessing the related hazard at Vesuvius and Campanian Plain (Sandri et al., this issue).

The structure of the work consists of an integrated geological, geomorphological, stratigraphic and sedimentological study, a paleomagnetic and sediment-mechanic impact assessment calculation, and a comprehensive discussion on the lahar problem in the Campanian Plain.

2. Geological setting

The study area is part of the Campanian Plain, which includes the lowlands surrounding Mount Vesuvius volcano and the nearby Apennine ridges and valleys (Fig. 1). The orography of the area is characterized by three WNW-ESE trending mountain ridges that border eastward the plain, with an elevation ranging from 500 to 1600 m a.s.l., and slope angles from 30 to 60°. From north to south, the Avella-Partenio, Lauro-Visciano and Sarno-Quindici mountain ridges are separated by two depressions: the Avella-Baiano Valley, in which the alluvial plain of the Clanio river occurs, and the Lauro valley. Both are narrow valleys that widen toward north-west, among the cities of Cicciano, Nola and Palma Campania (Fig. 1). The reliefs are characterized by a high drainage density, associated with a poorly developed and torrential hydrographic network, which over time has favored the incision and dismantling of the pyroclastic cover on the ridges, and the development of numerous detrital conoids that connect with the main valley floor (Di Vito et al., 1998).

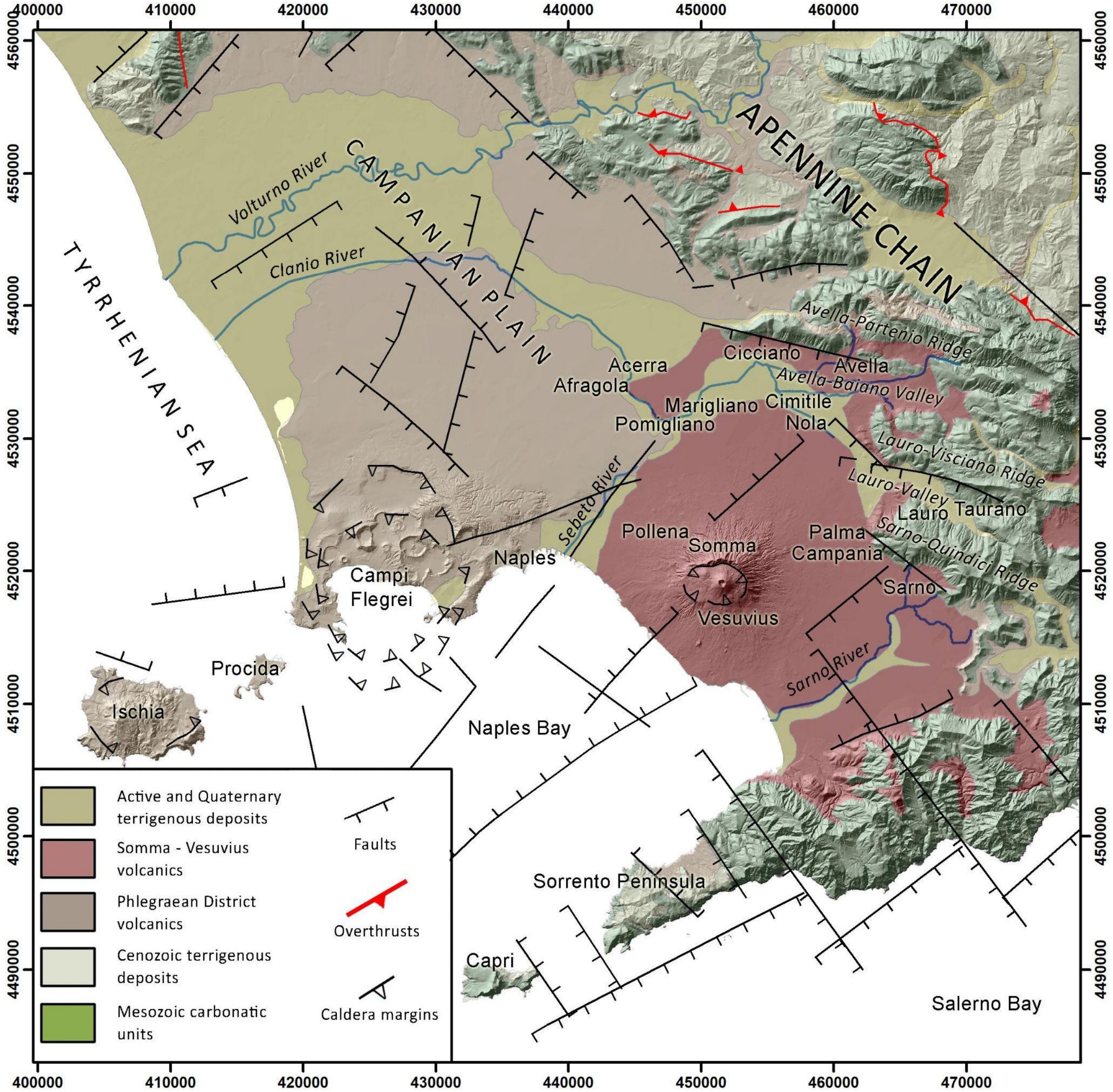

Fig. 1. Geological and structural sketch of the Campania Region on a Shaded Relief derived from TINITALY DEM. The coordinates are expressed in WGS 84 UTM N33 (modified after Orsi et al., 1996).

Vesuvius, or more properly Mt. Somma-Vesuvius, is a composite central volcano less than 39,000 years old, composed of the remnant of the oldest Mt. Somma edifice, dismantled by repeated episodes of caldera collapse, and the more recent Mt. Vesuvius, grown inside it. Its volcanic history is characterized by an initial phase, dominated by low-energy effusive and explosive eruptions, which ended at around 22,000 years ago. Since then, the volcano generated four Plinian eruptions with VEI

5-6, each preceded by long periods of quiescence and all accompanied by a summit caldera collapse (Somma caldera; Cioni et al., 1999). The last Plinian eruption occurred in 79 CE and once again modified the Somma caldera, inside which the recent cone has subsequently grown due to an alternation of periods of open conduit, persistent Strombolian and effusive activity, and long periods of quiescence with obstructed conduit, interrupted by high-energy sub-Plinian eruptions. In historical times, the other more energetic events were the sub-Plinian 'Pollena' (472 CE) and 1631 eruptions (Santacroce et al., 2008). The last eruption occurred in 1944 and caused the return to obstructed conduit conditions, which characterize the current quiescent phase of the volcano. The rocks composition varies from slightly silica-undersaturated (K-basalt to K-trachyte) to highly silica-undersaturated (K-tephrite to K-phonolite). The Somma-Vesuvius complex is characterized by a well-developed radial drainage network, which feeds an extensive volcaniclastic apron that morphologically connects the edifice with the surrounding plain (Santacroce et al., 2003). It represents the active southern termination of the Plio-Quaternary volcanic chain that borders the eastern Tyrrhenian margin (Peccerillo, 2003). Volcanism in this margin is related to the extensional tectonic phases that accompanied the anticlockwise rotation of the Italian peninsula, during the complex interaction between the Africa and Eurasian plates, which generated the Apennine thrust-and-fold belt (Ippolito et al., 1973; D'Argenio et al., 1973; Finetti and Morelli, 1974; Bartole, 1984; Piochi et al., 2004; Patacca and Scandone, 2007; Vitale and Ciarcia, 2018). The extension along the Tyrrhenian margin of the Apennine chain was accommodated by the activation of NW-SE normal faults and NE-SW normal to strike-slip transfer fault systems, which dismembered the chain in horst and graben structures, and allowed magmas to reach the surface and feed the volcanism (Mariani and Prato, 1988; Faccenna et al., 1994; Acocella and Funiciello, 2006). The Campanian Plain is one of these grabens that hosts the Neapolitan volcanic area. It is a NW-SE elongated structural depression, filled by a thick sequence of marine and continental sedimentary deposits, and volcanic-volcaniclastic successions that compensated its subsidence, leading to a complete emersion at around 39 ka (Brocchini et al., 2001; De Vivo et al., 2001; Santangelo et al., 2017). This graben is bordered toward

NW, NE and SE by the Meso-Cenozoic carbonate and terrigenous successions of the Apennine chain, and is subdivided in minor NE-SW oriented horst-and-graben structures (Carrara et al., 1973; Finetti and Morelli, 1974; Fedi and Rapolla, 1987; Brancaccio et al., 1991). Neapolitan volcanoes lie on these second-order structural highs (Marotta et al., 2022 and reference therein), and the products of their most powerful eruptions blanketed the Apennine reliefs and filled their valleys with several meter-thick covers of pyroclastic fall deposits, composed of pumice lapilli and ash layers separated by paleosols (Pareschi et al., 2002; Bisson et al., 2007; Cinque and Robustelli, 2009; Gurioli et al., 2010).

In terms of water drainage, the pyroclastic cover has peculiar geotechnical characteristics, such as a positive correlation between grain-size and permeability, which enabled the development of lahars in the area. In particular, coarser pumice layers are characterized by inter-clast void spaces that control water accumulation, instead ash layers, soils and paleosols by a high water retention capacity (Andosol-like soils), so that the differential behavior can regulate equilibrium among deposits stability vs. remobilization (Fiorillo and Wilson, 2004).

Regarding the volcanic activity of Vesuvius in the last 2,000 years, the largest eruptions after the 79 CE Plinian one were two sub-Plinian eruptions, the 472 CE Pollena and 1631 ones, but several other effusive and explosive events occurred in historical times. In the Campanian Plain, lahar deposits related to these two eruptions are quite abundant due to past heavy rains (Fiorillo and Wilson, 2004; Zanchetta et al., 2004b; Stanzione et al., 2023), also the sub-Plinian scenario is of interest for civil protection purposes, which is why in the present work we focus on the 472 CE Pollena and 1631 eruptions. A particular attention is given to the distribution of the primary pyroclastic deposits and related syn-eruptive lahars, which are mass flow events directly related to specific eruptions, even if the condition is not necessarily that of an event contemporaneous to the eruption. Those deposits are mainly composed of >90% fragments from the parental eruption, while the remaining fragments pertain to other eruptions mixed by volcaniclastic colluvium (Sulpizio et al., 2006). The syn-eruptive feature is thus related to the remobilization of pyroclastic deposits more than to the exact timing of lahar emplacement, the latter being of the order of max a few years (before humification processes or significant human activities can occur). Such a feature distinction is important because directly related to volcanic hazard.

3. Materials and methods

3.1. Evidence from historical sources

We collected data from historical sources, maps, documents, and newspapers to supplement the geological data, gathered directly or indirectly, for the definition of the areal distribution of the syn-eruptive and post-eruptive lahar deposits at Vesuvius and in the surrounding region. Such collection concerned the phenomena that took place starting from the sixteenth century CE to 2005. This time span has been chosen depending on data availability, and to show the high recurrence of events over time in the area. The data were collected and grouped not only by years but also by the municipal areas existing at those times. It should be noted that the distribution of the data can be affected by the different urbanization over time, and by the presence of damage to people, infrastructures and goods, economic activities and settlements. In the absence of local weather data series over the analyzed period, we assumed that the phenomena of remobilization of the pyroclastic deposits, and the consequent generation of large flooding events and volcaniclastic mass flows, coincided with extreme weather events often described and reported in the analyzed sources. We identified about 500 individual reports, covering events between the sixteenth century CE and 2005 that took place in 97 different municipalities. The data were organized in a geospatial database, so that it was possible to define different areas affected by frequent syn-eruptive floods and lahars, concomitant/related with the sub-Plinian eruption of 1631, to be used as benchmark for the main geological analyses. We could not add the Pollena eruption to this historical data set, as there are no available sources for similar occurrences other than documents deriving from archaeological excavations (see next sections).

The municipalities with the highest number of reports are: Sarno (43), Salerno (32), Siano (26), Vietri sul Mare (22), Bracigliano (21), Nocera Inferiore (20), Maiori (19), Quindici (17) (Fig. 1). The events of greatest intensity, which affected more than five municipal territories at the same time, are 19. Some of these occurrences result closely connected with the volcanic events of Vesuvius, such as those that occurred in 1631, 1823, 1910, 1949 and 1954, simultaneously or within months to a few years after the Vesuvius eruptions of 1631, 1822, 1906 and 1944.

Eruption	Lahar/Intense Alluvial Event	Municipalities affected
December 1631	16/12/1631	Sant'Anastasia, San Giorgio a Cremano, Massa di Somma, Somma, Ottaviano, San Sebastiano, Trocchia, Torre del Greco, Portici, Pugliano, Madonna dell'Arco, Palma, Nola Arpaia, Arienzo, Cicciano, Marigliano, Benevento, Avellino
October 1822	24/01/1823	Amalfi, Bracigliano, Cava de' Tirreni, Cetara, Minori, Nocera Inferiore, Pagani, Salerno, Sant'Egidio del Monte Albino, Tramonti, Vietri sul Mare
	12/02/1823	Maiori
	12/04/1823	Sarno
	18/10/1823	Corbara, Praiano, Sant'Egidio del Monte Albino, Sarno, Siano
	15/11/1823	Salerno
April 1906	24/10/1910	Amalfi, Boscotrecase, Cercola, Cetara, Ercolano, Giffoni Valle Piana, Maiori, Marano di Napoli, Minori, Napoli, Pollena Trocchia, Torre del Greco, Vico Equense, Vietri sul Mare, Sant'Anastasia, San Giorgio a Cremano, Sarno, Scala, Pomigliano d'Arco, Portici, Ravello, Salerno
March 1944	02/10/1949	Lauro, Maiori, Minori Nocera Inferiore, Sarno, Vietri sul Mare
	25/10/1954	Cava de' Tirreni, Maiori, Minori, Nocera Inferiore, Salerno, Tramonti, Vietri sul Mare

Tab. 1. Historical archive of lahar and alluvial events related to the four most significant Vesuvius eruption in the last four centuries, and municipalities affected by such events.

The absence of information in the Lauro and Avella-Baiano valleys is likely due to the absence of detailed descriptions of alluvial events, or most likely to the position of the inhabited areas generally located on the hills thus far from the lower part of the valleys. The investigated area was affected many times by post-eruptive lahar events due to the presence of thick variably-weathered pyroclastic deposits mantling the steep slopes of Somma-Vesuvius and Apennines. One of the most recent event occurred on May 5th 1998, when a 16-hours prolonged heavy rainfall triggered a huge number of Apennine slope failures toward the towns of Quindici, Bracigliano, Siano, Sarno and San Felice a Cancello, all located near the Apennine ridges east-northeast of Somma-Vesuvius (Fig. 1). This catastrophic event involved an extension area of around 60 km^2, and a volume of more than $2x10^6$ m^3 (40% derived from materials eroded along the channels), causing 160 victims and severe damages to the quoted towns (Di Vito et al., 2019 and references therein).

3.2. Field and archaeological investigations

We used a set of geological, stratigraphical, sedimentological, archaeological, and pedological information for the reconstruction of the type of events, their emplacement mechanisms, timing, and impact on pre-existing structures/environment. Such an approach enabled us to cross-check geological and archaeological evidence allowing us to accurately fix the age of events. Conversely, the presence of well-dated primary pyroclastic deposits can define the age of human traces otherwise not easily datable. Furthermore, the identification of the "primary" (fallout and pyroclastic current, along with the archeological findings) can give the absolute age (*ante* or *post quem*) of a given deposit. The definition of isochronic paleosurfaces can also contribute to the reconstruction of the paleo-environments affected by the deposition, and of the variations that occurred during depositional processes. For this purpose, particular attention was paid to the basal contacts between the deposits. In some areas like Nola (10-15 km from Apennine source valleys), the lahar deposits directly overlie the primary pyroclastic deposits (both for the 472 CE Pollena and 1631 eruption), while in other areas some pyroclastic units or the whole primary deposits are missing (eroded) or lacking. Only the correlation with the nearby areas permitted to define whether the emplacement of the lahars eroded partly or significantly the underlain primary deposits, vice versa the complete absence in the emplacement areas could also be due to the distribution of these latter. The analysis of the internal structure marked by sharp changes in grain sizes, color, presence of erosional unconformities, or interposition of lenses of coarser material also permitted the identification of one or more flow units within the same individual deposit package. The macroscopic characteristics of the sequences permitted some inferences on the transport and depositional mechanisms, while the grain-size and componentry analyses provided information on the source deposits that were remobilized. This brings to another important definition, that is syn-eruptive vs. post-eruptive lahars, according to the definition of Sulpizio et al. (2006) and Iverson and Vallance (2015), which applies during or soon after the eruption vs. several years to centuries after the eruption ended, respectively. The macroscopic analysis allowed us to distinguish between the syn-eruptive and post-eruptive deposits. The first ones are defined by the occurrence of pyroclastic components with a lithology similar to the one of the primary deposits. The second ones are characterized by some evidence of depositional stasis like humified paleosurfaces below the lahar deposits or of anthropogenic activities, or by the presence of humified material and/or fragments of older eruptions in the deposits. All these characteristics allowed the correlation between the various volcaniclastic units for the whole set of the studied sequences, marking the differences needed to hypothesize on the source and invasion areas.

We reviewed all the volcanological and archaeological data collected during the last 20 years from drill cores, outcrops, archaeological excavations, and from the existing literature, in collaboration with colleagues of the Archaeological Superintendence of Campania region. The preliminary collection and analysis of the existing data permitted to plan a hundred of new stratigraphic trenches (Fig. 2), with the aim of collecting stratigraphic, sedimentological, lithological and chronological data on the primary pyroclastic and secondary (lahar) deposits. Particular attention was also paid to the geometric relations of these deposits with the paleotopography and preexisting anthropogenic structures.

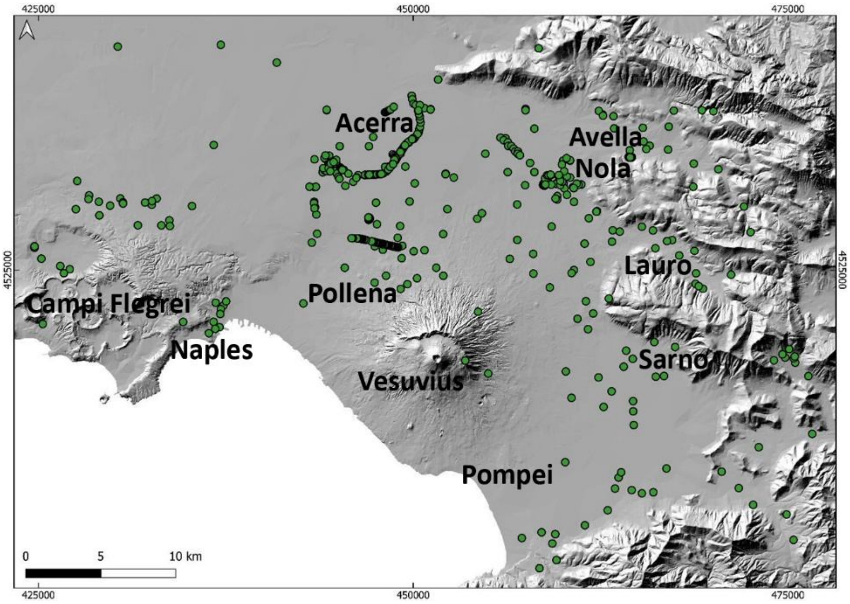

Fig. 2. Shaded relief of the studied area and location of all the sites where stratigraphic analyses were carried out.

The collected data were organized into a geospatial database (QGIS Platform), in which each point represents an investigated site linked to a series of information, such as the precise location, type of volcanic sequence, and stratigraphic features (primary and secondary units, thickness, type of deposit, etc…). The data were visualized using a Digital Elevation Model (DEM) of the Campanian Plain as reference topography and the UTM WGS 84 – Zone 33N reference projection.

3.3. Geomorphological analysis

This analysis is aimed at identifying the macro-basins that fed the lahars in the study area after the two sub-Plinian eruptions (Pollena and 1631). The analysis was carried out on the basis of the slopes distribution and the watersheds extracted from a Digital Elevation Model (DEM). The DEM was derived from a LiDAR flight of 2012 (cell size of 10 m). In particular, six macro-basins characterized by slopes > 20° were identified in the Somma-Vesuvius area, whereas fifteen macro-basins with slopes > 25° were identified in the Apennines to the East of the volcano (Fig. 3). The different slopes thresholds are defined starting from previous studies (Pareschi et al., 2000, 2002; see also Bisson et al., 2013, 2014), and on the basis of a better analysis of the physical characteristics of the remobilized material, in turns related to the various types of deposits. In fact, on the steep slopes and in the valleys of Somma-Vesuvius the deposits are mainly ash-rich pyroclastic current deposits and subordinately lapilli fallout deposits, while on the Apennines they are ash and lapilli fallout deposits. Each basin was considered as a single feeding unit for the lahars generation, and this is an input for the modeling of possible future lahars in the companion papers (de' Michieli Vitturi et al., this issue; Sandri et al., this issue).

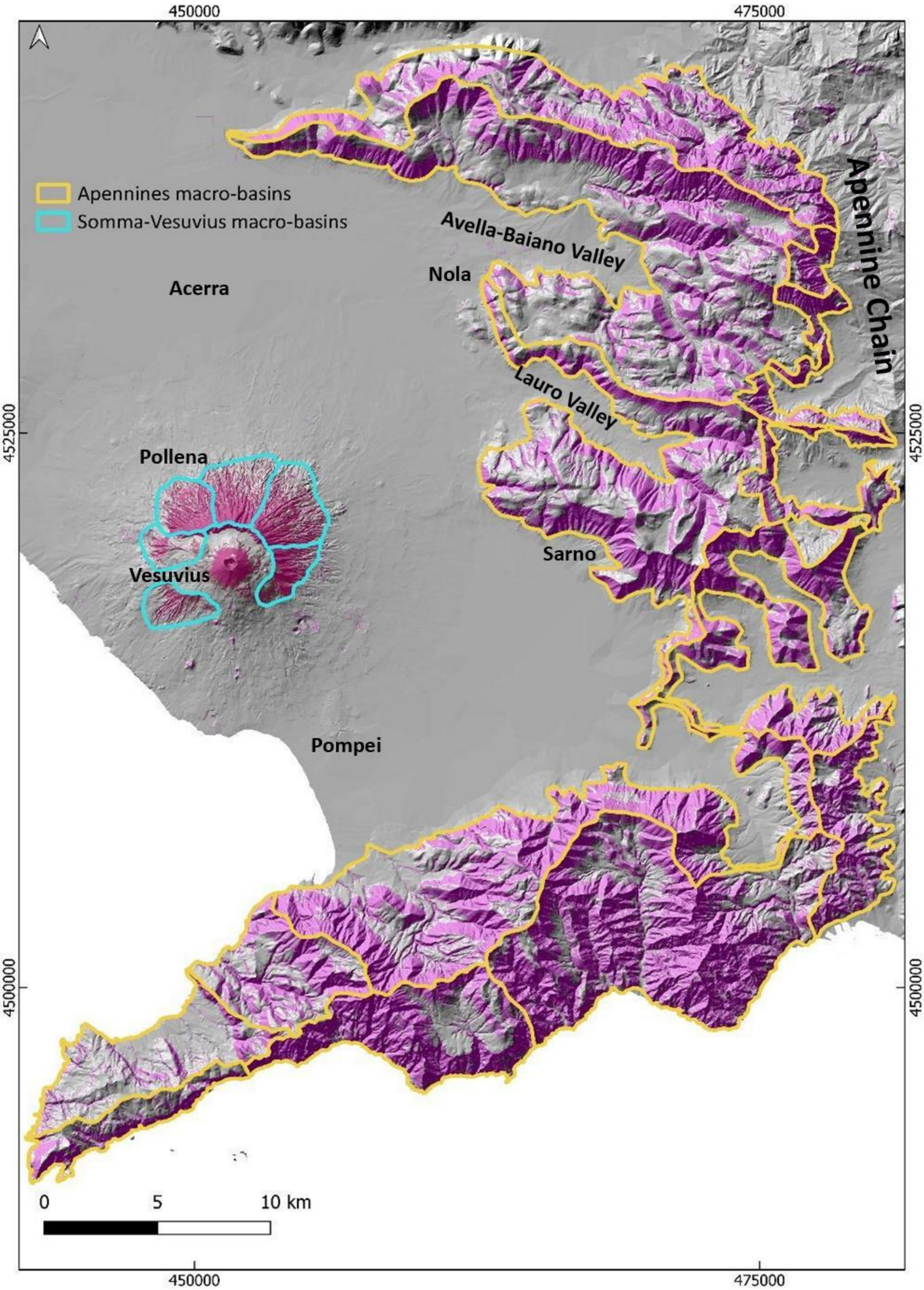

450000
475000
Apennines macro-basins
Somma-Vesuvius macro-basins
Avella-Baiano Valley
Apennine Chain
Nola
Acerra
Lauro Valley
4525000
Pollena
Vesuvius
Sarno
Pompei
4500000
0
5
10 km

304

Fig. 3. The macro-basins defined on the basis of their geomorphological features to study the areas of possible accumulation and mobilization of deposits, which are used in modeling lahar generation of future events.

3.4. Laboratory and analytical work

3.4.1. Grain-size

In selected studied sites reported in Fig. 4, macroscopic analyses of the stratigraphic sequences were carried out in the field to first identify any homogeneities or similarities between the juvenile fraction of the primary and secondary deposits, and then recognize the various volcaniclastic units. This was followed by sampling the deposits and carrying out the laboratory analyses.

In particular, the sampling was mostly made on the syn-eruptive lahar deposits, but also on the post-eruptive and, in a few cases, on the primary pyroclastic deposits. All lab analyses were performed in the laboratories of sedimentology and optical microscopy at the Istituto Nazionale di Geofisica e Vulcanologia, Sezione di Napoli Osservatorio Vesuviano (INGV – OV). The material samples were pre-heated at a temperature of 60-70 °C to eliminate any fraction of humidity, then were quartered and sieved. To avoid any breaking of fragile clasts like pumices, the dry sieving of the grain-size classes between -4 (a coarse limit variable depending on the sample) and 0 phi was made manually, while for the classes between 0.5 and 5 phi a mechanical sieving apparatus was used.

In particular, the fine ash-rich deposit samples with a high degree of cohesion (with a significant amount >0 phi) were diluted in distilled water, then boiled to remove all ash aggregates, before being analyzed for grain-sizes following a wet procedure, and finally dried and weighted by classes. The cumulative class >5 phi was further separated by interpolation modelling (de'Michieli Vitturi et al., this issue). In the post-processing of the data, the GRADISTAT excel package by Blott and Pye (2001) was used to determine the main statistical parameters. On selected samples, a microscopic componentry analysis was performed, consisting of recognizing and separating the various lithotypes that compose the volcaniclastic deposits, that is juvenile, lithic and crystal clasts. The clasts recognition was made manually for the coarser fractions, while for the finest fractions it was necessary the use of a reflected-light binocular microscope.

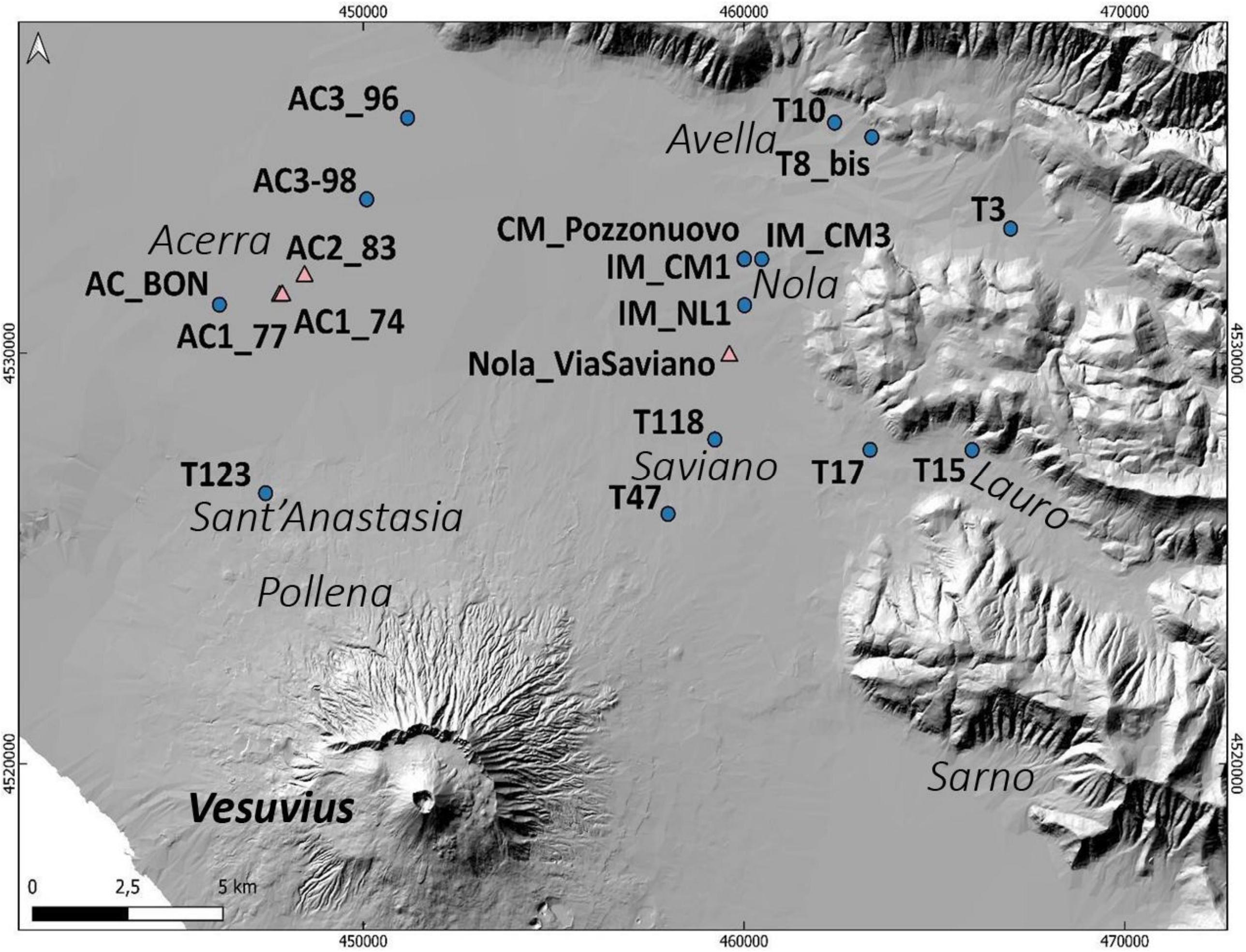

Fig. 4. Location of sites in which the sampling was carried out for sedimentological and paleomagnetic analyses. The pink triangles represent the sites for which a paleomagnetic study was carried out (AC1_74, AC1_77, AC2_83, and Nola_Via Saviano). In several sites, multiple samples were taken at different stratigraphic heights; samples labeled with US were taken at CM_Pozzonuovo site (see results).

3.4.2. Input for impact parameters

A significant number of large clasts and boulders was also found embedded in the lahar deposits at different locations. These clasts have dimensions from several centimeters to several tens of centimeters in diameter, and their nature is variable, that is limestone, ceramic, brick, tephra, lava, sandstone, iron (in order of abundance). Most of the clasts are fragments of artifacts from buildings, structures, and other archaeological finds of the Roman period, and their shape can be approximated in the field to ellipsoid. All these features suggest that they were entrained from substrate into the lahars to ultimately be deposited together with the main finer solid load of the lahars. In the dynamics of volcaniclastic mass flows like lahars and pyroclastic currents, the occurrence of boulder entrainment by flow dynamic pressure is recognized as a quite common feature (e.g., Zanchetta et al., 2004a; Pittari et al., 2007; Duller et al., 2008; Toyos et al., 2008; Cas et al., 2011; Carling, 2013; Doronzo, 2013; Jenkins et al., 2015; Roche, 2015; Martí et al., 2019; Guzman et al., 2020). The capability of a flow to entrain a clast is a function of flow properties (velocity, density) and clast properties (dimension, density, shape), and dynamic pressure well syntheses and quantifies such capability also in terms of flow hazard (Toyos et al., 2008; Zuccaro and De Gregorio, 2013; Jenkins et al., 2015). In Appendix A, a theoretical scheme is presented to invert these field features for calculation of the impact parameters at local scale.

3.4.3. Rock magnetism

The lahar deposits related to the Pollena eruption were analyzed by rock magnetism in the municipalities of Acerra (12 km from Somma-Vesuvius) and Nola (10-15 km from 10-15 km from Apennine source valleys) at four localities (Fig. 4), where the lahars interacted with anthropogenic structures. At each locality, we collected oriented samples, then measured about 200 specimens. We sampled both the deposit matrix and some potsherds embedded along three trenches (74, 77 and 83) and in the "Nola-Via Saviano" excavation. The purpose of the magnetic measurements was threefold: i) evaluating the magnetic fabric of the deposits to infer the local to regional flow directions of the lahars and possibly their origin, whether from the Apennines or Vesuvius. The magnetic fabric in this type of deposits records the main flow direction (local/regional) followed during the emplacement processes; ii) estimating the deposition temperature (T_{dep}) of the deposits, to understand whether the lahar was triggered soon after the eruption or at later times. The hypothesis is that the temperature is higher in case of syn-eruptive lahars deriving from hot (pyroclastic current) deposits, and lower in all other cases; iii) testing the relative sequence (contemporaneity) of the lahars emplacement with respect to the Pollena eruption. All hand-samples were oriented *in-situ* with magnetic and solar compasses and reduced to standard sizes at the CIMaN-ALP laboratory (Peveragno, Italy), where all the magnetic measurements were made. In Appendix B, the adopted paleomagnetic techniques and nomenclature are described.

4. Results

4.1. Field stratigraphy and sedimentological features

In this study, data of about 500 sites were collected, covering an area of >1000 km^2 from the plain around the volcanic edifice to the Apennine valleys to the north and east (Fig. 2).

4.1.1. Pyroclastic deposits: Pollena and 1631 eruptions

The integration of the collected data with the existing ones (Rosi and Santacroce, 1983; Rosi et al., 1993; Rolandi et al., 2004; Sulpizio et al., 2005; Perrotta et al., 2006; Bisson et al., 2007; Santacroce et al., 2008; Gurioli et al., 2010; De Simone et al., 2011) allowed the reconstruction of the distribution maps for both the fallout and pyroclastic current deposits. In particular, the spatial distribution highlights that for both the Pollena and 1631 primary deposits, thick fine ash deposits are widely distributed and cover the coarse fallout sequence or directly the ground, modifying the isopachs reconstructed by previous authors (Sulpizio et al., 2006 and references therein; Figs. 5 and 6). This enlargement of the area affected can have important implications on the hazard evaluation in terms of possible damages on a densely inhabited territory.

The area covered by the comprehensive isopach maps (including both lapilli and ash fallout) turns out to be wider than previously known, above all because we took into account for the ash fallout occurred during the final phreatomagmatic stages of the eruptions (Rosi and Santacroce, 1983; Sulpizio et al. 2005). The great availability and distribution of these ash deposits could explain the wide generation and distribution of the syn-eruptive lahars in the area. This has important implications on the evaluation of the source area and material available for the lahars accompanying and following these eruptions. Interestingly, there is an increase of the areas covered by pyroclastic deposits. The QGIS recalculated 10-cm isopach area covered by the fallout deposits is of 837 km^2 (Pollena eruption) and 528 km^2 (1631 eruption), which compared to the lower values of 569 km^2 (Pollena eruption) and 158 km^2 (1631 eruption) after Sulpizio et al. (2006) give an extra surface of about 47% and 230%, respectively. Geotechnically, another implication is that the wide presence of fine and cohesive ash, not only on top of the coarse fallout sequences but also on the ground, preventing water infiltration, favoring surficial runoff and creating sliding surfaces (Baumann et al., 2020).

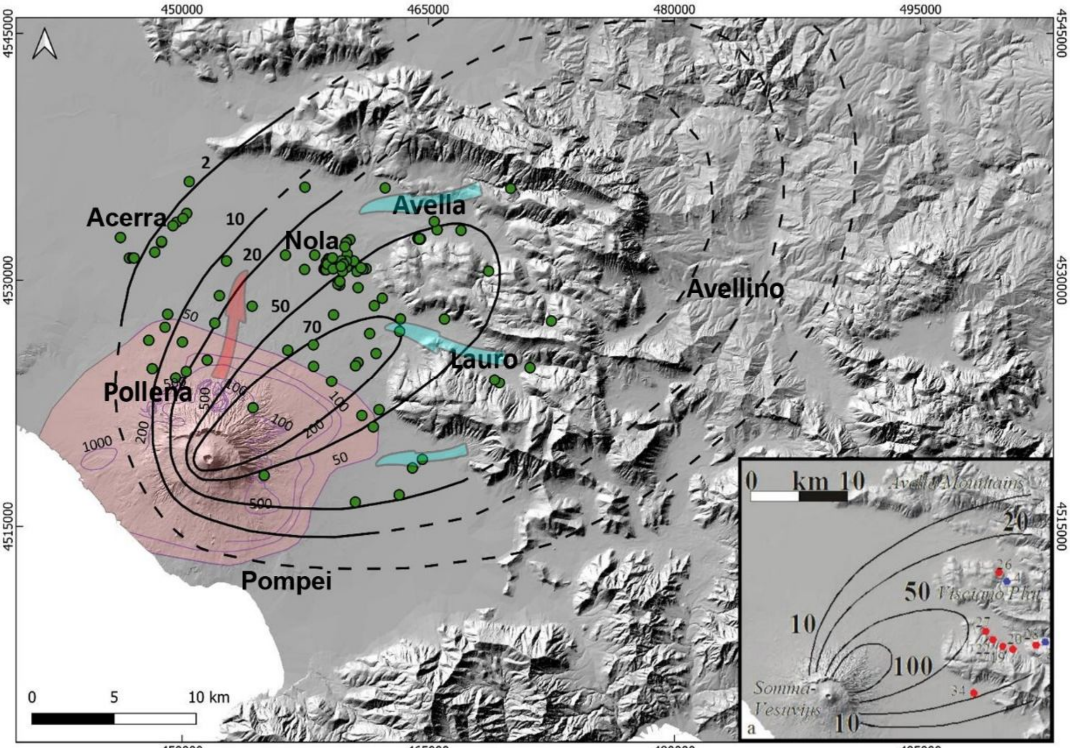

Fig. 5. Pollena eruption: the black lines represent the isopachs (in cm) of the fallout deposits modified after Sulpizio et al. (2006) (in the inset) on the basis of the new collected data (green dots), while in pink is colored the area affected by the pyroclastic current deposits (isopachs in cm, purple lines) modified after Gurioli et al. (2010). The dotted isopachs are extrapolated. The light blue arrows represent the general remobilization of the pyroclastic fallout deposits and lahar propagation from the Apennine slopes, while the pink one represents the combined remobilization of the pyroclastic current and fallout deposits and lahar propagation from Somma-Vesuvius.

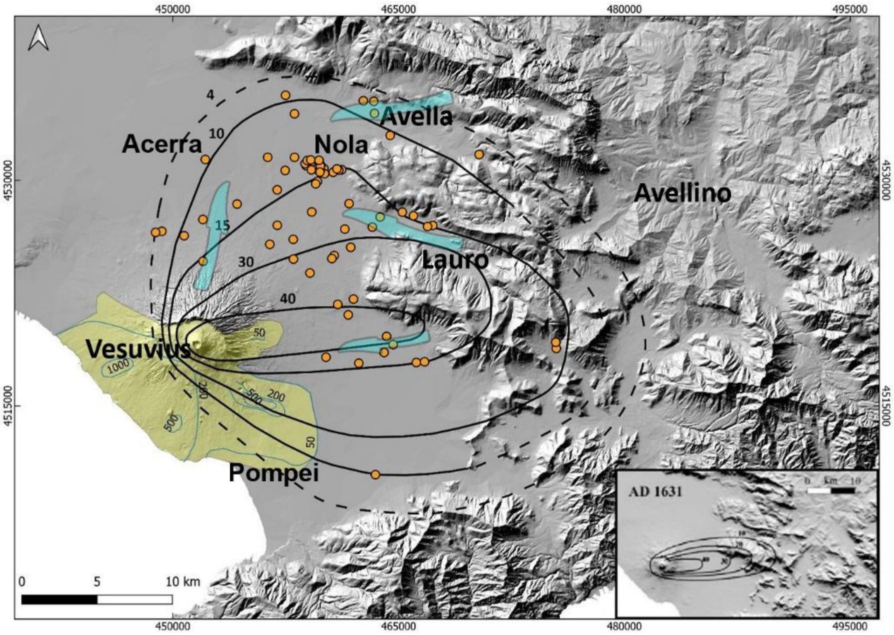

Fig. 6. 1631 eruption: the black lines represent the isopachs (in cm) of the fallout deposits modified after Santacroce et al. (2008) (in the inset) on the basis of the new collected data (orange dots), while in yellow is colored the area affected by pyroclastic current deposits (isopachs in cm, light blue lines). The light blue lines represent the inferred distribution on the basis of an integration between field data and chronicles modified after Gurioli et al. (2010). The dotted isopachs are extrapolated. The light blue arrows represent the general remobilization of the pyroclastic fallout deposits and lahar propagation from the Apennine slopes and Somma-Vesuvius.

The area affected by accumulation of the 1631 eruption tephra-fallout deposits is wider than previously known, particularly toward the north, which follows the inclusion of the final ash deposits into the new isopachs. Interestingly, such widening of the area agrees with the occurrence of lahars in the plain north of Vesuvius, as documented in the historical sources (Rolandi et al., 1993; Rosi et al., 1993, and references therein), and as follows.

4.1.2. Lahar deposits

The lithological and sedimentological analyses carried out in the field allowed the macroscopic definition of the primary pyroclastic deposits affected by the remobilization, and of the lahar deposits.

In many cases, the archaeological findings permitted to define the local paleoenvironment and related land use, then permitted to constrain the age and timing of the deposition.

We grouped all deposit descriptions into representative lithofacies to more directly characterize both the primary pyroclastic and lahar deposits (Tab. 2 and Fig. 7). Given the amount of data and description of the studied areas, we used these lithofacies to characterize a number of macro-areas between the Somma-Vesuvius sector and the nearby Apennine valleys (Appendix C).

Symbol	Lithofacies
P	Paleosol and humified surface, massive and composed of fine sand and silt from brown to dark brown, with several percentages of clay and organic matter. It indicates a stasis in the depositional processes.
mL	Alternation of massive lapilli layers. Pyroclastic fall deposit composed of pumice and scoria lapilli with sparse accidental lithics.
mA	Massive ash. Pyroclastic fall deposit composed of fine to coarse ash with sparse pumice fragments, scoriae and accidental lithics.
Gms	Massive gravel and sand deposit, matrix-supported and poorly-sorted. The matrix is composed of fine to coarse sand, while the gravel clasts comprise scoria and pumice clasts from the pyroclastic fall deposits. The massive feature of the single layers suggests a rapid emplacement from a highly-concentrated lahar.
mM	Massive mud deposit composed of fine sand, silt and clay, sometimes with sparse pumice and lithic clasts. It is generated from a mud-dominated lahar.
Sh	Horizontal lamination and bedding features in sands. The deposit is composed of an alternation of fine to coarse sand and gravel, which can be gradual or sharp. It comes from a hyper-concentrated lahar (less dense than the Gms one).
Ss	Scour and fill structures composed of fine to coarse sand, generally with a normal grading. A single structure consists of an erosive, concave upwards basal surface and a planar/convex top.
fM	Fine mud deposit composed of fine sand, silt and clay. It is generated when the lahar loses its energy and the fine grains settle gently.

Tab. 2. Symbol and description of the recognized lithofacies, and photos representative of each of them.

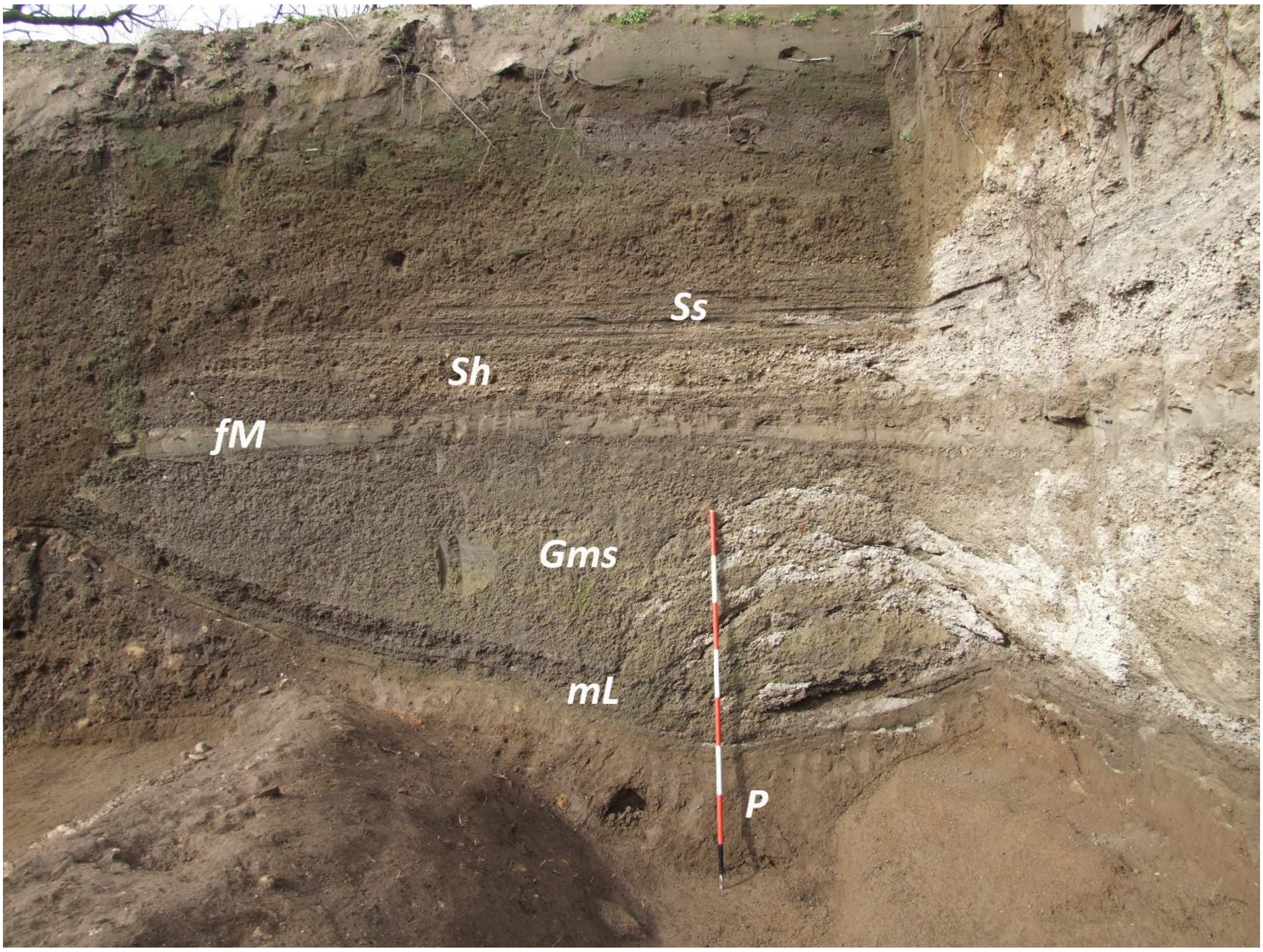

a)

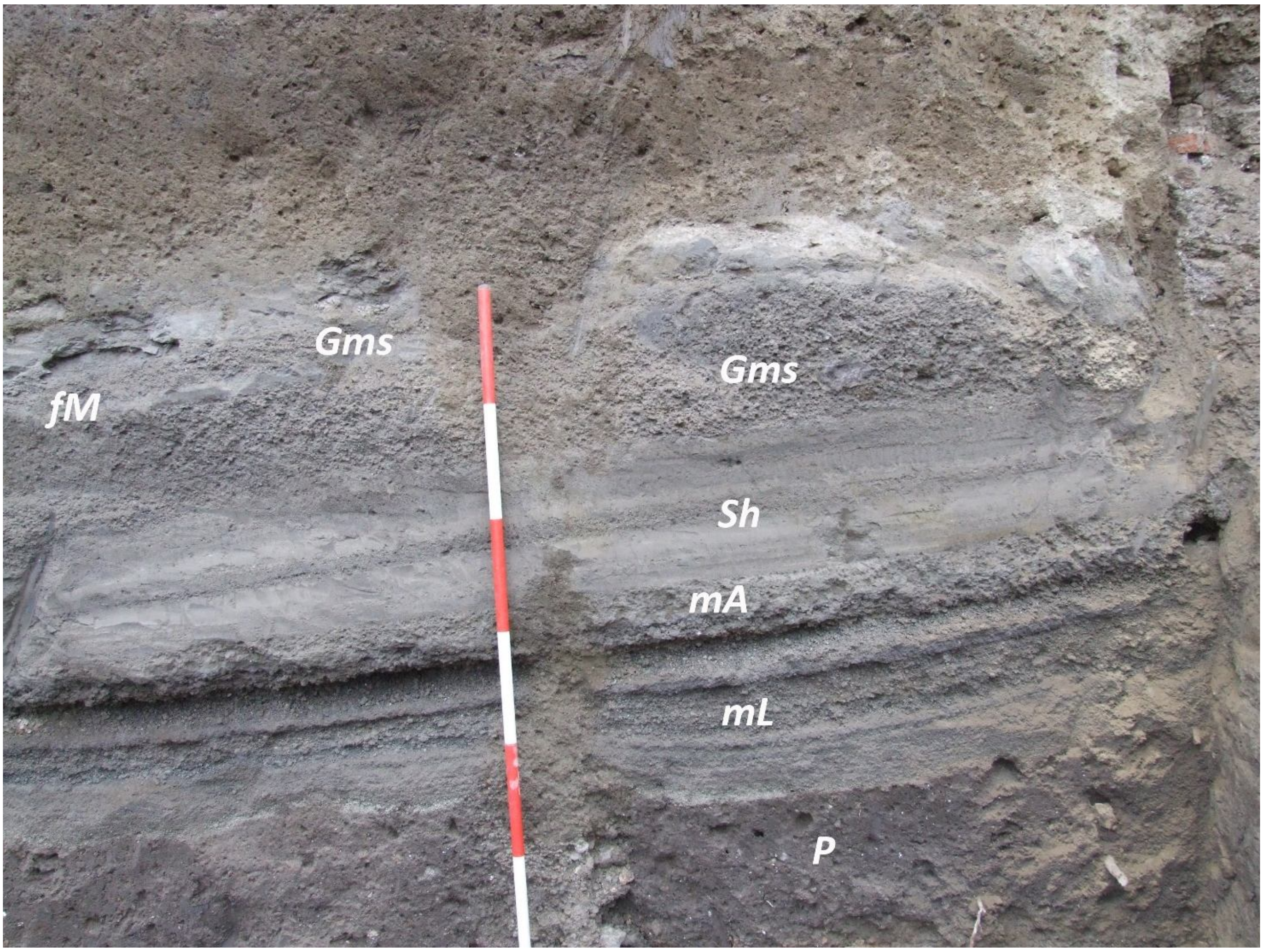

b)

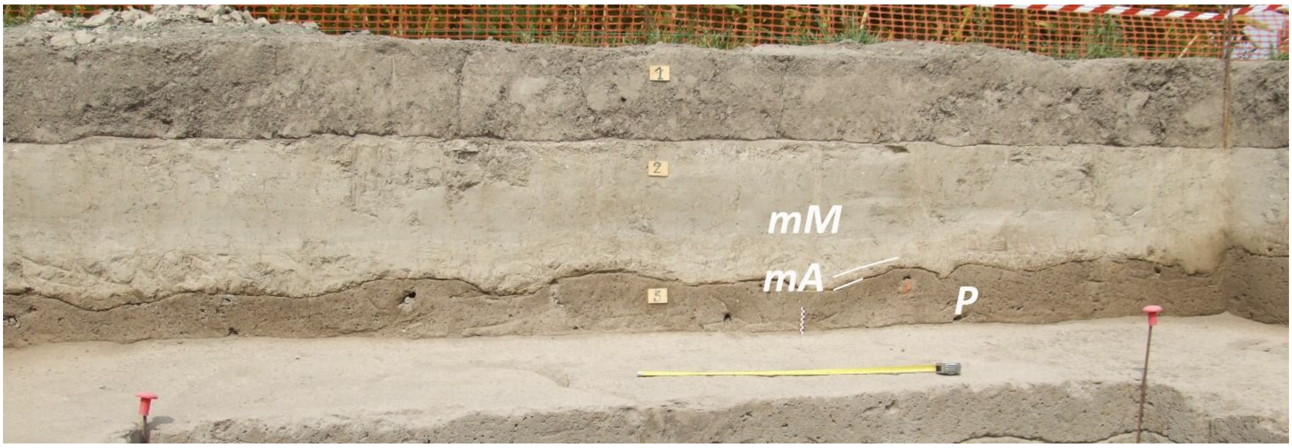

c)

Fig. 7. In these three photos of archaeological excavations (a-b, Nola at 10-15 km from Apennine source valleys; c, Acerra at 12 km from Somma-Vesuvius), the main lithofacies recognized in the field are shown, including paleosols, pyroclastic deposits, and lahar deposits; the corresponding lithofacies descriptions are reported in Tab. 2.

Usually, the syn-eruptive lahar deposits directly overlie the primary pyroclastic deposits, sometimes eroding them. They have a matrix-supported texture and are composed of fine to very fine cohesive ash, and contain more or less abundant cm-sized pumice and lithic fragments. In general, these deposits consist of multiple depositional flow units, each one resulting from single-pulse “en masse” emplacement, the piling of which resulting from rapid progressive aggradation through multiple flow pulses, in analogy with dense pyroclastic currents (Sulpizio et al., 2006; Doronzo, 2012; Roche, 2012, 2015; Breard and Lube, 2017; Smith et al., 2018; Guzman et al., 2020; see Sulpizio et al., 2014, p. 56). Consequently, the studied lahars were modelled using a shallow layer approach (de’Michieli Vitturi et al., this issue). The different depositional flow units in the same deposit are distinguishable (still in continuity) from each other based on vertical granulometric changes, sparse pumice alignments, deposit layering and/or unconformities. For example, compared to channelized pyroclastic currents, dense water flows and floods, such depositional units (layers) could have been repeatedly emplaced, from bottom to top, under accumulation rates of a few tens to hundreds kg/m^2s (Lowe, 1988; Russell and Knudsen, 1999; Whipple et al., 2000; Girolami et al., 2010; Roche, 2015; Marti et al., 2019; Guzman et al., 2020). In various areas, such rapid sequential emplacement is suggested by the presence of water escape structures through the whole deposit by crossing the sequence of several units. These are vertical structures consisting of small “pipes” filled with fine mud transported by the escaping water, and formed soon after the emplacement of the lahar units. The textural characteristics are variable even within the same site, but in general the deposits are massive and contain vesicles, from circular to flattened, coated by fine ash that adhered into the voids after water loss. For the syn-eruptive lahar deposits, the pumice fragments are those of the primary deposits. On the other hand, in the upper parts of the sequences it is not uncommon to find units that contain pumice fragments related to previous eruptions (9.0 ka B.P. "Mercato" and 3.9 ka B.P. "Avellino" Plinian eruptions), recognizable based on pumice texture and crystal content (Santacroce et al., 2008). In this second case, the lahar deposits are considered as post-eruptive, meaning that the pyroclastic deposits older than the two studied sub-Plinian eruptions were progressively involved in an advanced erosion of the slopes and valleys. The presence of slightly humified surfaces below the lahar deposits or the trace of human artifacts, such as for example excavations, ploughing, etc…, are considered as evidence of a long period without deposition; also in this case, the lahars are considered as post-eruptive. In other words, the similar componentry of the lahar and pyroclastic deposits, and the evidence of short-term exposure between these two, are strong indicators of the syn-eruptive occurrence of the lahar events. Instead, the absence of such features is more indicative of a post-eruptive origin, i.e. lahars events more spaced in time from the corresponding eruption.

In Appendix C, a description is reported for some of the most representative sequences, which were sampled in different areas throughout the plain (Figs. 2 and 4).

4.1.3. Distribution maps of the lahar deposits

Here we present distribution maps for the lahar deposits of the Pollena and 1631 eruptions (Figs. 8-11). The maps show the distribution of all thicknesses detected in the studied sites. In particular, the syn-eruptive Pollena lahar deposits are distributed in the NW quadrants of the volcano and in the Avella, Lauro and Sarno valleys (see Fig. 1), with a thickness exceeding 1 m in the Vesuvius apron and in the plain between Nola and Cimitile at about 10-15 km from Apennine source valleys (see Figs. 1 and 8). A volume estimation of the remobilized deposits is of the order of 7×10^{7} m^{3} for the northern Vesuvius area, and 4×10^{7} m^{3} for the Lauro Valley. Such volumes are referred to the depositional areas, and not to the detachment ones; for the latter see de'Michieli Vitturi et al. (this issue) and Sandri et al. (this issue). The provenance of the material in each site was inferred by sedimentological recognition and magnetic reconstruction. Then, the covered areas were subdivided into polygons in the geospatial database, in order to weight the local deposit thicknesses and estimate the volumes with a lower approximation.

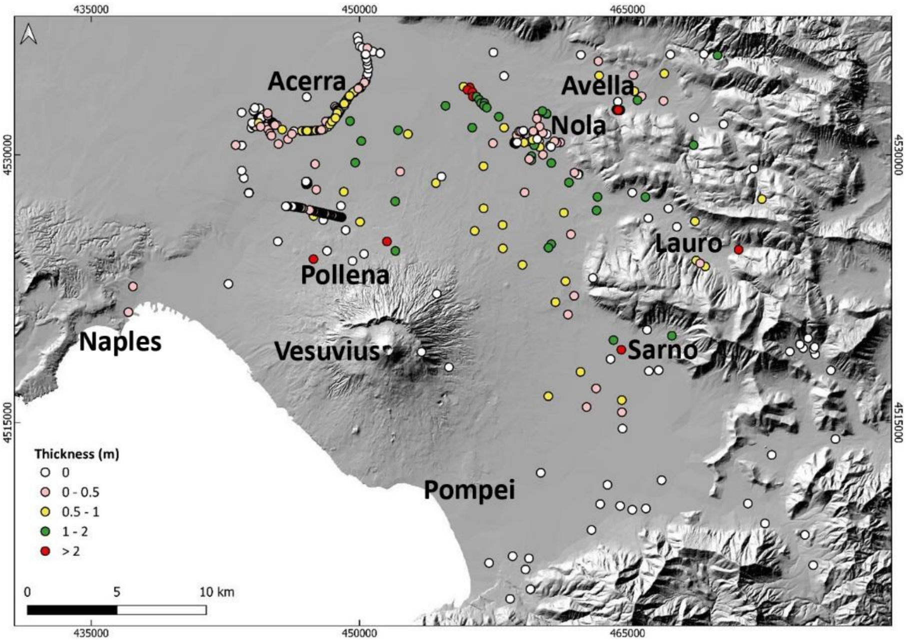

Fig. 8. Distribution of the syn-eruptive lahar deposits related to the Pollena eruption. The 0 m points represent the studied sites where the lahar deposits were absent, and in some cases even the primary pyroclastic deposits below were absent; they are reported anyway, as their absence might have not necessarily occurred by no deposition (local erosion).

The post-eruptive lahar deposits of the Pollena eruption are more distributed in the Avella and Lauro valleys, and in the plain north of the volcano close to the apron area (low-angle edifice outer slopes) (Figs. 1 and 9). Their deposits contain both fragments from the Pollena eruption and from preceding eruptions, suggesting that pyroclastic deposits of the older sequences were progressively eroded and involved in remobilization processes over time. As an example, on Fig. C1 it is to remark that whitish pumice fragments from the Pomici di Avellino and Mercato eruptions were identified on top of the Pollena lahar deposits.

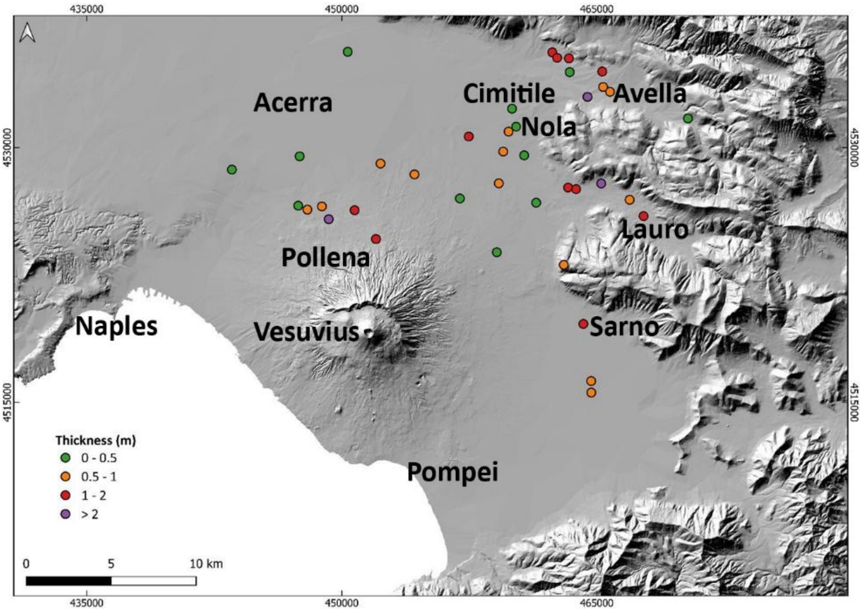

Fig. 9. Distribution of the post-eruptive lahar deposits related to the Pollena eruption.

The distribution of the syn- and post-eruptive Pollena lahar deposits is related to the primary pyroclasts deposition: the dense distribution of the lahar deposits north of Somma-Vesuvius depends on the presence of thick pyroclastic current deposits that were remobilized from the northern slopes of the volcano, while the distribution in the Apennine valleys is related to the fallout deposits that are thicker along the major Pollena dispersal axis (Fig. 5).

Above the Pollena pyroclastic and lahar deposits (both syn- and post-eruptive), the studied sequences in almost all the sites show the presence of a well-developed soil bed with many traces of cultivation, as well as of inhabited areas and buildings (Figs. C1-4). These traces and the presence of the soil bed are evidence of a progressive geomorphological stabilization of the territory. The occurrence of the 1631 sub-Plinian event determined a new phase of marked geomorphological instability for a large territory surrounding the volcano. In Fig. 10, it is shown the distribution of the syn-eruptive lahar deposits for the 1631 eruption in all the studied areas, having a variable thickness, generally <50 cm. Such distribution affected mostly the areas of Acerra-Nola, Sarno, the Vesuvius apron and the Apennine valleys (Figs. 1 and 10). Rosi et al. (1993) and Sulpizio et al. (2006) reported that floods and lahars heavily impacted (also with injuries and victims) the N and NE quadrants of Somma-

Vesuvius soon after the eruption with a timescale of days (Rosi et al., 1993; see also the historical chronicles of Braccini, 1632), corroborating the syn-eruptive behavior of such lahars. Some lahar deposits are intercalated within the primary pyroclastic deposits, but in general they directly stand on top of the pyroclastic deposits (Rosi et al., 1993); both cases unequivocally constrain the syn-eruptive behavior of the 1631 eruption lahars.

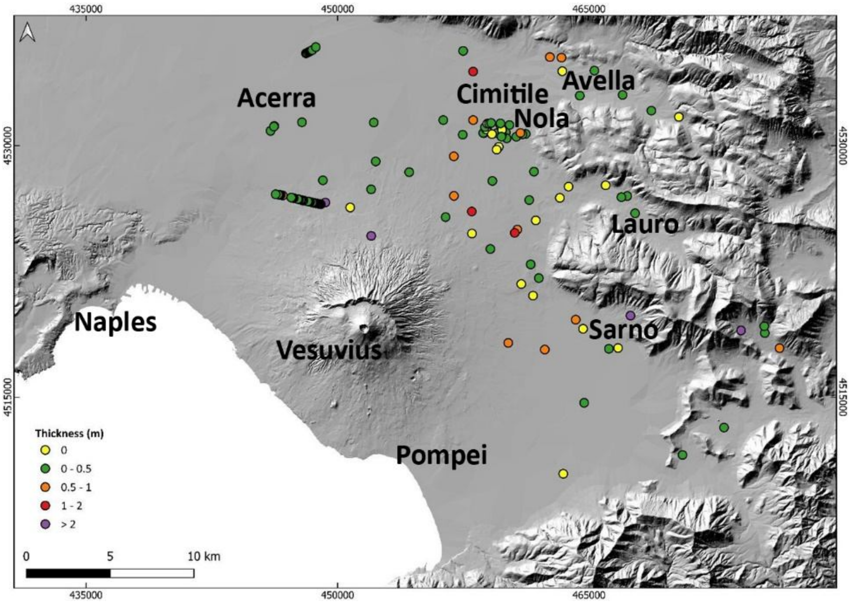

Fig. 10. Distribution of the syn-eruptive lahar deposits related to the 1631 eruption. The 0 m points represent the studied sites where the lahar deposits were absent, and in some cases even the primary pyroclastic deposits below were absent; they are reported anyway, as their absence might have not necessarily occurred by no deposition (local erosion).

In Fig. 11, minor post-eruptive lahar deposits of the 1631 eruption are reported, with a preferential distribution to the E quadrants of the volcano from N to S, both in the plain and the valleys. These deposits are still significant, with a thickness of around half a meter to a meter or more in a few points.

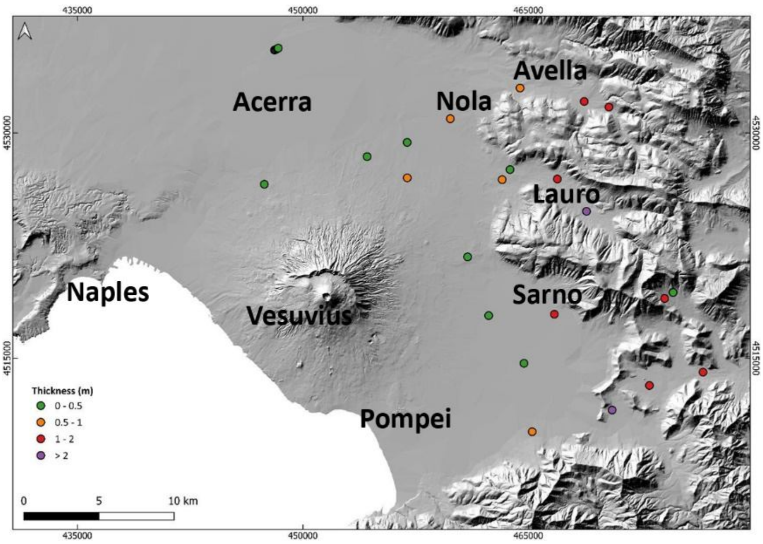

Fig. 11. Distribution of the post-eruptive lahar deposits related to the 1631 eruption.

The distribution of the syn- and post-eruptive 1631 lahar deposits mainly reflects the major dispersal axis affecting the fallout deposits distribution, while the pyroclastic current deposits were minorly remobilized as exposed on the gentler slopes of southwestern Vesuvius (Fig. 6).

4.1.4. Sedimentological characteristics of the Pollena lahar deposits

The field analysis was carried out in about 500 different sites for the construction of the database and maps, while the laboratory analysis was carried out on 30 samples representative of the different areas. The results of the grain-size analyses (cumulative curves and statistical parameters) are presented in Fig. 12 and Tab. 1.

Petrological analysis on the syn-eruptive lahar deposits have not been performed because the lithology (colour, texture, mineral content) of the components is the same as the juvenile material of the primary deposits described in Sulpizio et al. (2005). The loose crystals consist of sanidine, leucite, biotite and pyroxene fragments. Based on the results of the grain-size analyses, the coarser classes are defined from -4 to -1 phi, the medium ones from -0.5 to 2.5 phi, and the finest one from 3 phi. The juvenile pumice clasts are an ubiquitous component of the lahar deposits (both syn- and post-eruptive), but they decrease with distance for the finer grain-size classes, while the crystal content increases with the same progression. The lithic clasts are abundant for the coarser classes, they decrease with distance for the medium classes, and increase again for the finer classes.

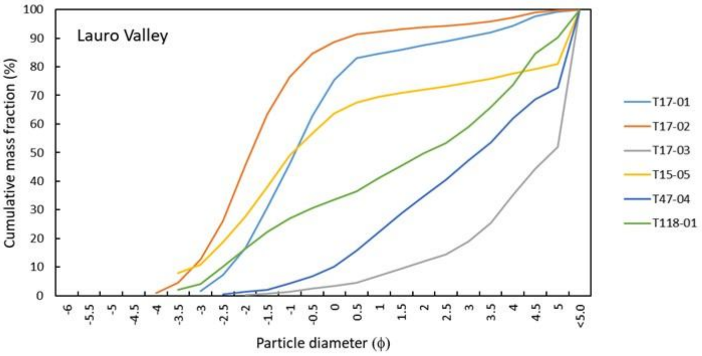

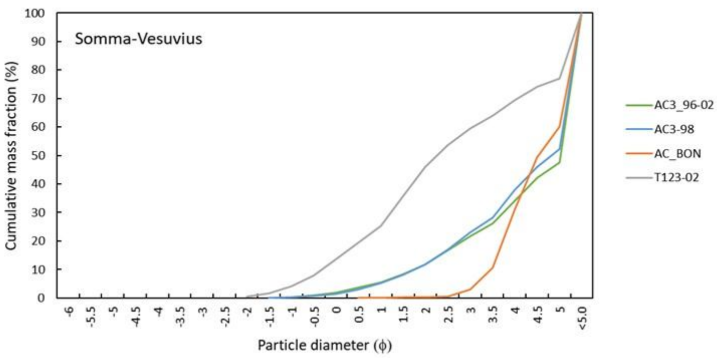

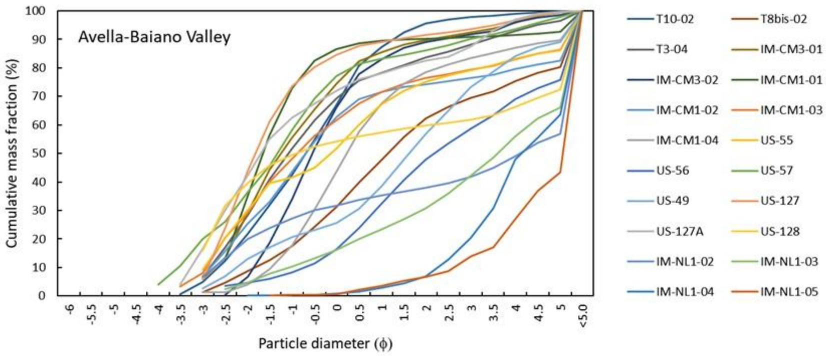

Fig. 12. Cumulative curves of the grain-size analysis on the samples taken at the locations reported in Fig. 4, and subdivided in three sectors: Lauro Valley (top), Somma-Vesuvius (middle), and Avella-Baiano Valley (bottom).

Sample	Mean (ϕ)	Sorting (ϕ)	Lithofacies
Lauro Valley			
T17-01	-0.93	1.41	Gms
T17-02	-1.83	1.23	Gms
T17-03	2.42	1.46	Sh
T15-05	-1.39	1.74	Gms
T47-04	1.67	1.61	Mm
T118-01	1.13	2.7	Gms
Avella–Baiano Valley			
T10-02	-0.78	1.47	Sh
T8bis-02	0.31	1.83	Sh
T3-04	-0.95	1.83	Gms
IM-CM3-01	-1.13	1.54	Gms
IM-CM3-02	-0.48	1.35	Gms
IM-CM1-01	-1.66	0.86	Gms
IM-CM1-02	-1.17	1.62	Gms
IM-CM1-03	-1.13	1.83	Gms
IM-CM1-04	0.06	1.39	Fm

US-55	-0.84	1.97	Gms
US-56	1.17	1.8	Sh
US-57	-1.51	1.86	Gms
US-49	0.69	2.16	Gms
US-127	-1.66	1.39	Gms
US-127A	-1.02	2.23	Gms
US-128	-1.72	1.91	Gms
IM-NL1-02	-0.5	2.49	Gms
IM-NL1-03	1.25	2.1	Gms
IM-NL1-04	2.99	0.89	fM
IM-NL1-05	2.64	1.20	fM
Somma-Vesuvius			
AC3_96-02	2.37	1.26	mM
AC3-98	2.48	1.2	mM
AC_BON	3.52	0.38	mM
T123-02	1.37	1.5	mM

Tab. 3. Statistical parameters (mean and sorting) extracted from the grain-size analyses, and reference lithofacies (see Tab. 2 for descriptions).

Field observations and grain-size analyses, highlight significant differences between the sectors of Lauro Valley, Avella-Baiano Valley, and Somma-Vesuvius. A common feature between the three sectors is that the lahar deposit samples are mostly massive, poorly-sorted and polymodal; only a few samples are moderately-sorted and unimodal (sorting <1.5 phi). On the other hand, the grain-size modes found show some interesting differences (in Fig. 12 the cumulative curves are shown). The coarse modes for Lauro Valley and Avella-Baiano Valley span from fine/medium lapilli to coarse ash, while for Somma-Vesuvius span from coarse to fine ash. The medium modes for Lauro Valley and Avella-Baiano Valley span from coarse to medium ash, while for Somma-Vesuvius span from medium to fine ash. The fine modes for Lauro Valley and Avella-Baiano Valley, and for Somma-Vesuvius span from medium to fine ash. All these differences basically depend on the origin of the primary pyroclastic deposits, fallout vs. pyroclastic currents, which were remobilized from different sectors, Apennines and Somma-Vesuvius. The grain-size analysis is used as an input information for the lahar transport model (de' Michieli Vitturi et al., this issue) aimed at assessing the related hazard (Sandri et al., this issue).

4.2. Magnetic results

Both Acerra (12 km from Somma-Vesuvius) and Nola (10-15 km from Apennine source valleys) localities show a well-defined magnetic fabric for the Pollena syn-eruptive lahar deposits. Principal susceptibility axes ($K_1 \geq K_2 \geq K_3$) are clustered. Magnetic lineation (K_1) and magnetic foliation (K_3, pole of the plane) are mostly sub-horizontal or gently embricated. The anisotropy degree P (K_1/K_3) is mostly lower than 1.060, but can reach high values like 1.200. At Acerra, the magnetic foliation is always dominant, and the fabric is oblate. The Pj is linearly correlated to the mean susceptibility (k_m). In Appendix B, the full nomenclature is defined for completeness. The magnetic fabric has a horizontal magnetic foliation and a clustered magnetic lineation, whose mean direction is NE-SW. Considering the chaotic nature of the lahar deposits, the high Pj and the clustered susceptibility axes can highlight a channelized flow (Fig. 13). At Nola instead, the fabric is both prolate/oblate, and Pj is lower than 1.040. The susceptibility axes are more dispersed than at Acerra, but mean magnetic lineation clearly shows a NW-SE direction. If one considers the oblate specimens only, the magnetic foliation is sub-horizontal, on the contrary, the magnetic foliation of the prolate specimens is steeply dipping (65°) toward SE. At Nola, the flow direction inferred by AMS is consistent and parallel to the invasion basin.

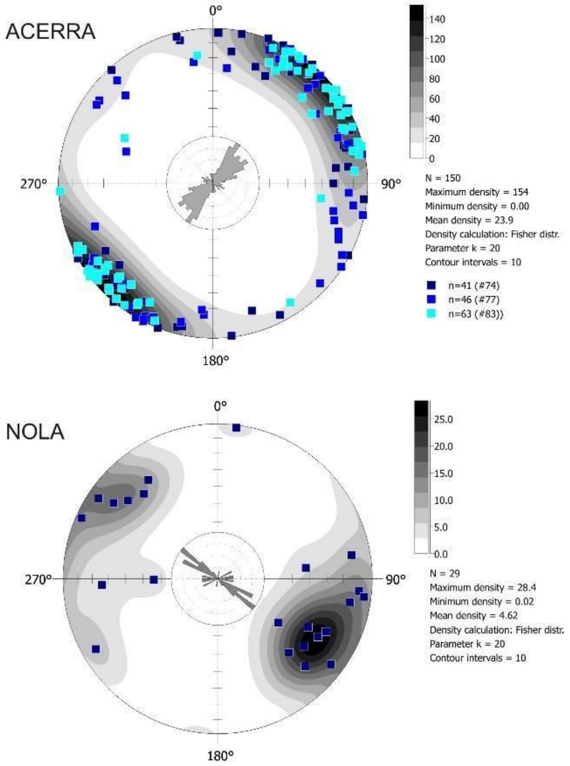

Fig. 13. Equal area projection and Rose diagram of the K_1 directions at Acerra (12 km from Somma-Vesuvius) and Nola (10-15 km from Apennine source valleys).

At Acerra, the T_{dep} interval is 120-140 °C, while for Nola T_{dep} is lower than 120 °C (Fig. 14). In the Nola case, a low temperature magnetization component lower than 120 °C cannot be directly considered as a TRM. In fact, the low T_b Earth's field component of magnetization can also be produced by a viscous remanent magnetization (VRM), acquired during exposure to weak fields (Bardot and McClelland, 2000). The acquisition of the VRM depends on the duration of the exposure. For age around that of the Pollena eruption, the minimum T_{dep} which can be distinguished is ca. 120 °C. For this reason, we considered the Nola lahar to be emplaced at low temperature.

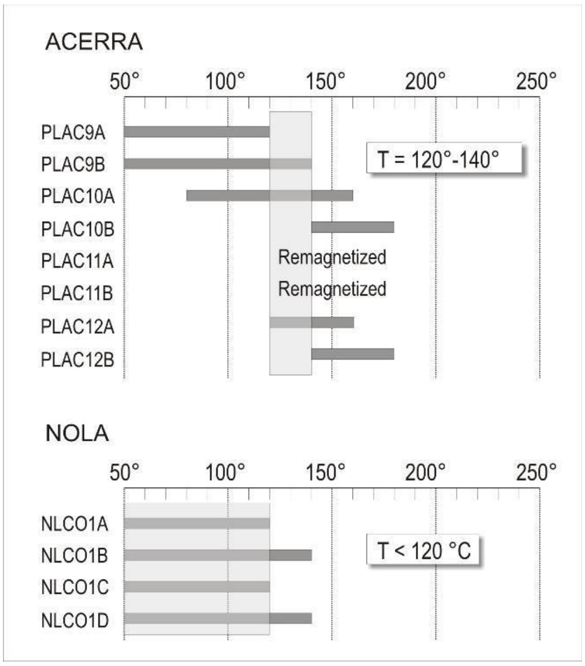

Fig. 14. Deposition temperature at Acerra and Nola. The site T_{dep} is estimated from the overlapping reheating temperature ranges for all lithic clasts sampled.

The mean paleomagnetic direction for each locality, calculated using Fisher's statistics, is well-defined, and its directional value and confidence limits do not overlap (Fig. 15). Thus, the two directions are statistically distinguishable at the 95% confidence limits. Since a paleomagnetic direction is a record of the Earth's magnetic field acting during the emplacement, it follows that the lahar deposits at the two localities are not synchronous.

Overall, all magnetic measurements just discussed show distinctly different characters between Acerra and Nola, clearly indicating two distinct events of emplacement.

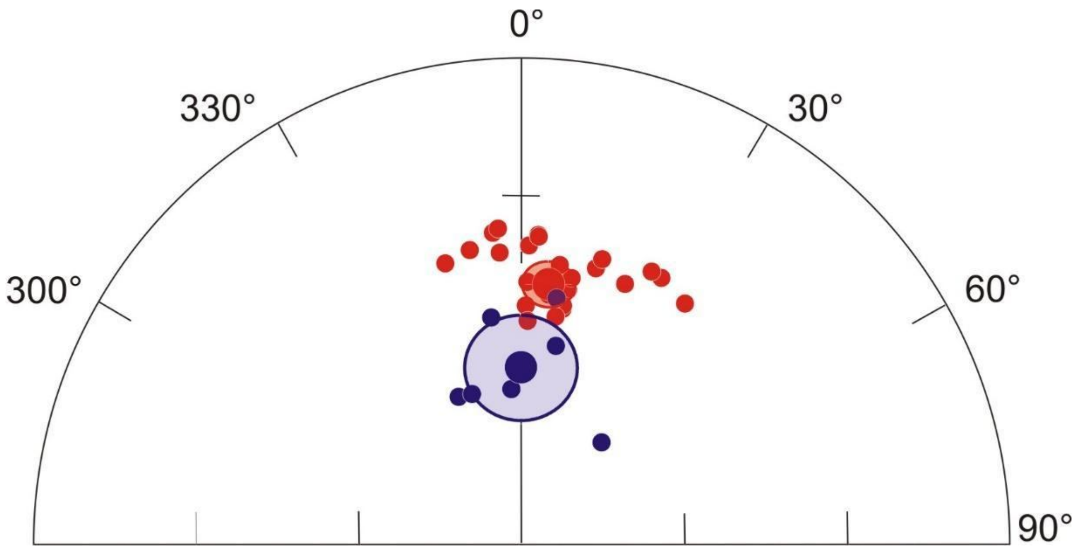

Fig. 15. Equal-area projection of the characteristic remanent magnetization directions, and their mean value with associated confidence limit, from Acerra (red dots, mean value: n=26 D=7.5°, I=43.4°, alpha95=3.5°), and Nola (blue dots, mean value: n=7, D=0.8°, I=60.2°, alpha95=9.0°).

4.3. Lahar dynamics

By inverting the field evidence and data, it is possible to reconstruct the macroscopic flow dynamics that occurred in the lahar invasion, which are particularly interesting to understand the impact that those lahars had on the Vesuvius territory. As already described, the lahar deposits show thicknesses that are variable from several centimeters to a few meters, and this can depend on multiple local factors: i) topography; ii) distance from source; iii) erosion; iv) source area and type of remobilized sediment (variably sized fallout vs. flow deposits). In particular, thicker deposits are found near the mouth of the valleys and in the flat alluvial plain, as shown in the deposit distribution maps. On the other hand, the deposits show a general tabular-like shape (Fig. 7), with an average thickness of the order of 0.5-1 m recurrent for several studied sites, which is the first evidence of the lahars impact and mass flow emplacement in the area. In terms of runout distance, the lahars travelled for 10 to 15 km from sources (Somma-Vesuvius and Apennine detachment areas), based on the geospatial database that includes all studied sites. It was possible to infer the source areas based on the common sedimentological features of the lahar deposits between nearby sites. On the other hand, distant sites with sedimentologically different deposits were fed from different source areas. These important constraints are used to validate and inform lahar numerical models (de’ Michieli Vitturi et al., this issue) and simulations (Sandri et al., this issue) using a shallow layer approach for hazard assessment. We cannot rule out that lahar pulses from different source areas (Somma-Vesuvius vs. Apennines) might have overlapped and further aggraded in the open plain.

At several locations, we found erosional unconformities (Fig. 16a) between the lower and upper flow units (Fig. 16b), as well as between the pyroclastic and lahar deposits. Erosion is an important factor for the entrainment of pre-existing materials and objects, which include large-size clasts external to the remobilized pyroclastic material. Size and density of the largest clasts embedded in the deposits can give an idea of the carrying capacity of the lahars.

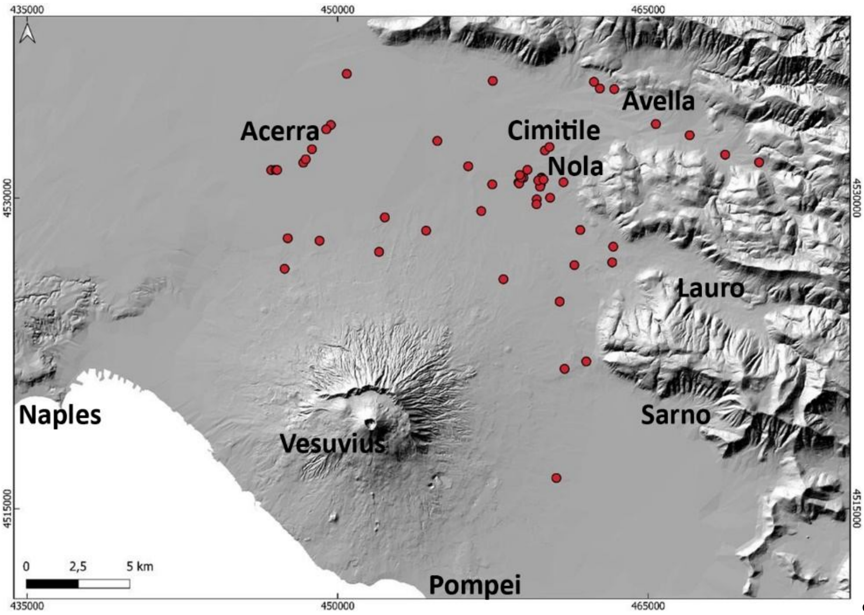

a)

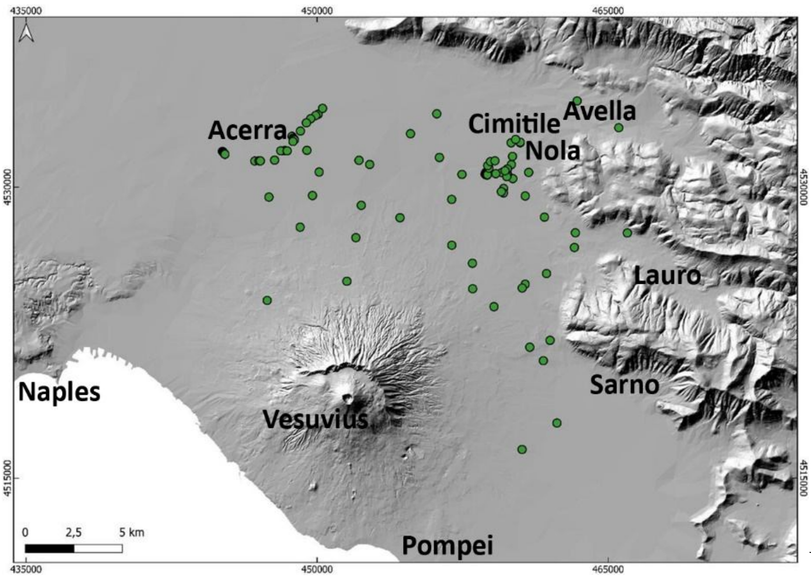

b)

Fig. 16. a) Sites with evident erosion traces at the base of the lahar units; b) Sites in which multiple depositional flow units are vertically identified. Both evidences corroborate the interpretation of the depositional mechanisms, as well as constrain the choice of the shallow layer approach for the lahar models and simulations (de'Michieli Vitturi et al., this issue; Sandri et al., this issue).

Occurrences of large clasts and boulders are reported in the area invaded both by the syn- and post-eruptive lahars, with a distribution that follows the one of the lahar deposits, in particular both are found at the mouth of the valleys and in the alluvial plain. The presence of the erosional features (Fig. 16a), and the fact that the deposits are mostly composed of massive and relatively thick units (Fig. 16b), suggest that high sediment transport and deposition both occurred in the same area (Doronzo and Dellino, 2013; Roche, 2015). Such occurrences of erosion and accumulation of multiple units were useful to inform the lahar modelling of de'Michieli Vitturi et al. (this issue).

We calculated local velocities of the syn- and post-eruptive Pollena lahars based on the biggest clasts that are found in the deposits at various stratigraphic heights, with boulder dimensions from several centimeters to a meter, and for flow density ≥ water density (Appendix A). The faster the lahar the higher the capability of its flow to entrain bigger external clasts. This occurred at locations where such clasts were freely available on the substrate, or where the lahars impacted and damaged anthropogenic structures.

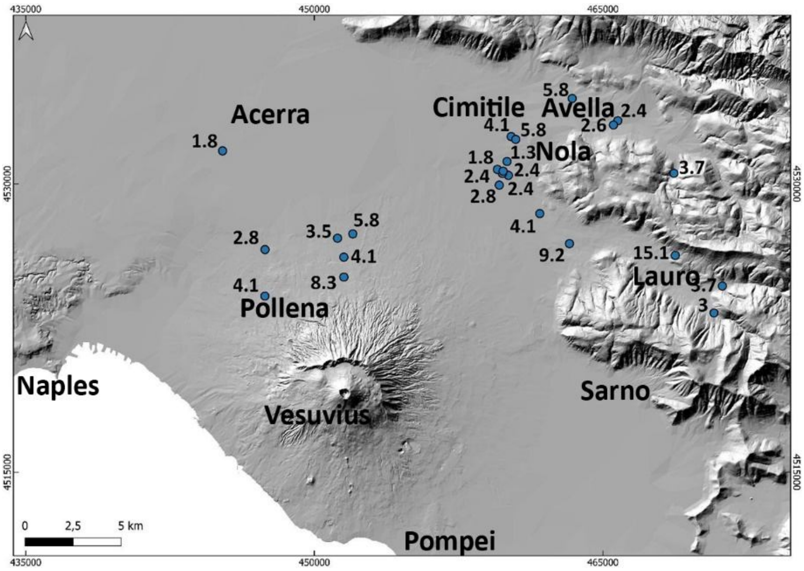

Fig. 17. Average lahar velocities (in m/s) estimated with a point-by-point reverse engineering approach.

Then, we used the flow velocities (Fig. 17) to calculate local dynamic pressures of the lahars (Fig. 18) as a function of the clast properties (size, density and shape). The obtained estimations are used by Sandri et al. (this issue) to validate the probabilistic hazard assessment of lahars from Vesuvius eruptions.

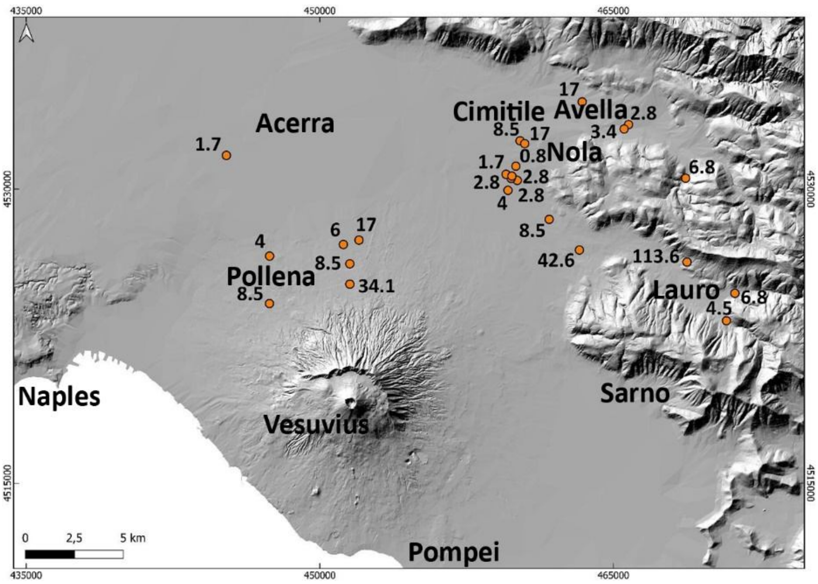

Fig. 18. Average lahar dynamic pressures (in kPa) estimated with a point-by-point reverse engineering approach.

The data presented in Figs. 17 and 18 represent minimum local values of the flow velocity and dynamic pressure, respectively, useful to assess some minimum impact of the lahars in the alluvial plain. An approximation of this point-by-point approach is that the values were calculated for the finding locations of the clasts in the deposits, meaning that the values are overestimated for those exact locations, while they should more properly be referred to the immediate surroundings upstream. We did a parametric test to quantify the sensitivity for different physical states of the multiphase flow depending on initial fluidization and flow density, and considering two end members, from a non-fluidized case to an initially fluidized and non-expanded case (see Appendix A; Roche et al., 2013). From the performed analysis, we found that the most typical values are referred to the initially fluidized and slightly expanded case (that is a few % more expanded than the non-expanded case), with most of the points falling in the range of velocity of 2-4 m/s, and dynamic pressure of 4-8 kPa. Lastly, in eight locations we found the lahar deposits emplaced against meter-sized obstacles, from which we estimated, by comparison, local flow heights of the order of 1-1.5 m, and particle volumetric concentrations of ~30% or more, i.e. the deposit thickness is ~1/3 of the lahar thickness (cf. Capra et al., 2018).

5. Discussion

The historical sources used as benchmark for lahars around Somma-Vesuvius and in the Apennine valleys remark the frequent and broad impact that explosive eruptions of Vesuvius had in historical times. Some of the eruptions in the last four centuries (e.g., 1631, 1822, 1906 and 1944) impacted on a number of municipalities, particularly during the sub-Plinian eruption of 1631. Heavy rain events caused remobilization of the primary pyroclastic deposits, triggering multiple lahars during or immediately after the eruption up to a few years (syn-eruptive lahars; Sulpizio et al., 2006); post-eruptive lahars were triggered on the longer term.

On the other hand, the Pollena eruption had an even wider impact, both in terms of primary pyroclastic deposition and secondary (lahar) impact. For this event, the historical sources are scarce to absent.

The analysis of – and realization of a database with – more than 500 stratigraphic sections were done, which also includes the sedimentological features of the lahars deposits relative to the two sub-Plinian Vesuvius eruption case-studies, Pollena and 1631. The detailed reconstruction and mapping of the primary deposits allowed to update the area affected by pyroclasts dispersal, and it was found that both eruptions had an impact larger than previously known. In particular, the stratigraphic and sedimentological reconstruction of the deposits was done not only in the countryside but also close to urban areas, and this is important in terms of local impact of the lahars in the environment. Specifically, such impact investigation was done in urban areas including archaeological findings (e.g., urban structures, walls, etc…).

These findings include not only new data from the Somma-Vesuvius plain, but also more distal data from Lauro Valley and Avella-Baiano Valley (Apennines), which were subjected to heavy remobilization of the primary deposits including the widely-dispersed fine ash deposits formed in the late stage of the eruptions. Indeed, the accumulation areas that were reconstructed reveal an enlargement and extra 47% (Pollena eruption) and 230% (1631 eruption) coverage that was not previously known, and this should be considered in the hazard and impact evaluation in the Campanian plain and on the nearby Apennine reliefs. The full database allows a more precise reconstruction of the new isopachs, both for the Pollena and 1631 eruptions, which is possible given the high number of data points in the study area.

With particular reference to the lahar deposits, the syn-eruptive ones occurred by relatively short-term (during or immediately after the eruption) events, and were directly emplaced on the primary pyroclastic deposits, both for the Pollena and 1631 eruptions. Also, there are not any significant erosion surfaces nor humification traces in the sequences due to prolonged exposure of the primary deposits, testifying that the secondary emplacement was quite immediate (max a few years; Sulpizio et al., 2006) after or even during the eruption. The syn-eruptive features are also testified by the absence of anthropogenic traces or humified surfaces at the base of or interbedded in the lahar deposits, as further evidence of a very short-term time span between the eruptions and the lahar events. Another interesting feature is the presence of multiple depositional flow units, as evidenced by grain-size changes, some clast alignments and concave erosion surfaces in the lahar deposits. Such depositional units were formed by en-masse emplacement (with reference to single flow pulse), while the whole lahar deposits were formed by rapid progressive aggradation of the various flow units (Vallance and Scott, 1997; Doronzo, 2012; Roche, 2012; Smith et al., 2018; Martí et al., 2019; Guzman et al., 2020; see also Sulpizio et al., 2014, p. 56), which does not contradict the principle of superposition. This can be argued by the generally massive facies of each flow unit in the deposits, and by the presence of water escape structures that cross vertically the entire deposits sequences. The latter evidence testifies a rapid water loss through vertical escaping "pipes" during or soon after the aggradation of the sequences. In other words, the various flow units (layers) must decouple from the transport system, and such decoupling occurs unit-by-unit and not particle-by-particle (Sulpizio et al., 2006, 2014; Roche, 2012; Doronzo and Dellino, 2013; Breard and Lube, 2017; Smith et al., 2018), through a massive accumulation rate (Duller et al., 2008; Doronzo et al., 2012; Martí et al., 2019).

The analysis of the Pollena lahar lithofacies allowed the identification of two main deposit categories. The first one occurs on an area that extends for more than 10 km north of Mount Somma, and the second one occurs on an area that extends west of the Apennines. For the latter, we can recognize two significant sub-categories of deposits, corresponding to the main valleys in northwest-southeast direction, Avella-Baiano Valley and Lauro Valley. The difference between the first and the second deposit categories seems to reflect the type of primary deposits that were remobilized (fine ash vs. ash and lapilli). In the area north of Mount Somma, which also comprises the municipalities of Acerra and Afragola (about 12 km from Somma-Vesuvius), the primary lapilli fallout deposits are absent. In this part of the plain, the thin layer of phreatomagmatic ash is widely present, while thick fine-grained pyroclastic current deposits are present in the Mount Somma valleys that fed some of the lahars. In

Avella-Baiano Valley and Lauro Valley, which also comprise the municipalities around Nola at 10-15 km from Apennine source valleys(Fig. 1 and Appendix C), the lahar deposits are generally coarser, and consist of multiple depositional units with different lithofacies (Tab. 3). In this case, both grain-size and componentry indicate that lahar deposits resulted from the remobilization of the fallout deposits. Such considerations also derive from the full compilation of the geospatial database. A volume estimation of the remobilized syn-eruptive deposits, based on a QGIS calculation, is of 7×10^7 m^3 for the northern Vesuvius area, and 4×10^7 m^3 for the Lauro Valley.

Referring to the 1631 eruption, previous maps have shown the distribution of the 1631 lahar deposits toward east, basically following the distribution of the primary pyroclastic fall deposits (Sulpizio et al., 2006), while in Figs. 10 and 11 we show a significantly larger distribution area particularly toward the north (Somma-Vesuvius ramps and plain) and east (Apennines valleys), and less toward the southeast. In particular, this distribution is well explained by the wide distribution of the ash fallout deposit toward both north and northeast (Fig. 6), remobilized during the lahar generation both from the Mount Somma and Apennine slopes. On the other hand, looking at the average deposit thicknesses, they reach half a meter in the north and northeast, while reach a couple of meters in some locations in the northeast (aligned with the dispersion axis of the primary fallout deposits and out of the Apennine valleys).

The sedimentological analyses carried out on a number of samples from the different studied sectors (Somma-Vesuvius, Lauro Valley, Avella-Baiano Valley) are useful for discriminating the various factors that contributed to the initiation of the lahars and emplacement of their deposits. The samples from Lauro Valley and Avella-Baiano Valley are coarser (but have a significant finer tail) than the ones for Somma-Vesuvius, and this can depend on three factors: i) genetic types of the primary pyroclastic deposits (fall vs. flow); ii) interaction between lahars and morphology (valley vs. plain); iii) major remobilization in Lauro Valley and Avella-Baiano Valley of the distal phreatomagmatic fine ash deposits formed in the late eruption stages. In other words, the primary grain sizes involved in the remobilization (finer and higher-water retention for Somma-Vesuvius), as well as the general topography (gentler but longer ramp for Somma-Vesuvius) likely acted as the main factors directly impacting the distribution of the lahar deposits, and the decay of the flow velocities and dynamic pressures in the area.

Interestingly, an emplacement temperature of ~120 °C of the lahar deposits was calculated for those generated along the Somma-Vesuvius slopes, indicating a relatively hot provenance after remobilization of the pyroclastic current deposits. Instead, the remobilization from the Apennines sectors involved only cold fallout deposits. The companion paper of de'Michieli Vitturi et al. (this issue) investigates also the nexus between water temperature, flow viscosity, and their consequential impact on fluid dynamics. Specifically, when the dominance of frictional forces is attributable to the yield slope term, the initial divergence between high- and low-temperature scenarios appears negligible. However, discernible dissimilarity appears over time for the inundation area of the colder flow case (i.e., 27 °C) with respect to the warmer counterpart (i.e., 100 °C), the latter case being close to the 120 °C one reported from paleomagnetism. Remarkably, the temperature-induced variations assume a pivotal role in shaping the dynamic characteristics of the hotter flow. The diminished viscosity associated with elevated temperatures not only amplifies fluid mobility but also prompts a notable acceleration in sediment settling velocity. This, in turn, initiates a debulking mechanism, thereby intensifying overall flow mobility. Consequently, this intricate interplay contributes to a reduced footprint of deposited material from the flow, altering the spatial distribution of sediments. However, the overall impact on the inundation area is typically quite reduced, being typically less than 10-20% even considering a thickness threshold of 1 mm (see de'Michieli Vitturi et al., this issue). The sampled clasts might have been incorporated multiple times by the flows, and the heating/cooling processes that we interpret as indicating T_{dep} in the diagrams are the last to have occurred and affected the samples. Besides, a third heating component is clearly observed for some of them. The paleomagnetic directions are statistically distinguishable, supporting that the lahar emplacement at

Nola (10-15 km from Apennine source valleys) and Acerra (12 km from Somma-Vesuvius) was not synchronous, as further evidence of the different timing hence likely different detachment areas involved during the pyroclasts remobilization. However, the comparison with the paleosecular variation curves of the Earth's magnetic field does not allow to better constrain the entity of the time span between the two lahar events. The parental lahars acted as mass flows capable of entraining outsized clasts (where available) from substrate under the action of shallow-layer flow velocity and dynamic pressure (de'Michieli Vitturi et al., this issue), then emplaced massive flow units with uplifted external clasts set into the much finer matrix (see Roche, 2015). In some lahar units, various clasts have been found, showing some alignment that depends on the mechanisms of entrainment and uplift (with respect to substrate) within the flow.

In terms of local impact in the Pollena case study (the largest one), while most of the calculated points (44) fall in the range of lahar velocity of 2-4 m/s and dynamic pressure of 4-8 kPa, a few peak values of velocity of 13-15 m/s and dynamic pressure of 90-115 kPa are also calculated, which are directly related to meter-sized clasts entrained into the lahars on the steep slopes, then deposited downstream of alluvial fans. Such values of the velocity and dynamic pressure are well comparable with those calculated for lahars that occurred recently at Ruapehu in 2007 (Lube et al., 2012) and Merapi in 2011 (Jenkins et al., 2015), and in historical times at El Misti (Thouret et al., 2022). In particular, the estimated velocities and pressure agree with those of Lube et al. (2012) and Jenkins et al. (2015). Moreover, multiplying velocity and density gives a power per unit surface, so those most representative values correspond to a flow power per unit surface of $8 \cdot 10^3$ - $3.2 \cdot 10^4$ W/m^2, with peak values of $1.17 \cdot 10^6$ - $1.72 \cdot 10^6$ W/m^2, in agreement with typical values reported for floods and megafloods (Russell and Knudsen, 1999; Whipple et al., 2000; Carling, 2013).

6. Conclusions

The integration of the historical, stratigraphic, sedimentological, laboratory, and impact parameter analyses carried out in the Vesuvius area allow us updating on the lahar invasion related to the Pollena and 1631 eruptions. In general, the physical characteristics of the analyzed deposits indicate that syn-eruptive lahars are related to the rapid remobilization of large volumes of pyroclastic material, which is mainly fine-grained and almost exclusively derived from the accumulation of products related to a single eruption. The analysis also shows that tardive (post-eruptive) mass flows are common, and involve multiple and variably altered deposits, and that their energy and frequency are progressively lower over time, after the last eruption has occurred. In particular, a higher impact both from primary and secondary phenomena is something that should be accounted in the Vesuvius area and that:

i) The new isopach maps of the Pollena and 1631 eruptions allow us to infer a larger impact than previously known for these two sub-Plinian events of the Vesuvius. Thus, it is worth reconsidering the territorial impact that sub-Plinian eruptions can have in the Vesuvius (but not only) area. In particular, the ash deposits can have a high impact in relation to their high density and low permeability.

ii) The primary impact from fallout and pyroclastic current processes in the Vesuvius area was - and may be in the future – followed by the secondary impact from lahars generated during or immediately after the eruption events. Both impacts can have a wide distribution, because they are directly controlled by the primary deposits distributions, both around Somma-Vesuvius and in the Apennines valleys.

iii) The runouts of such lahars were significant both for the Pollena and 1631 eruptions, by reaching distances of 10 to 15 km from the sources, and their deposits geometry is tabular-like with average thicknesses of 0.5 to 1 m.

iv) The paleotemperature data highlight a relatively hot dynamics (~120 °C) for those lahar flow pulses that traveled down the Somma-Vesuvius slopes because of pyroclastic current deposit remobilization. This did not occur from the Apennines sectors, where pyroclastic currents did not get to, and only cold fallout deposits were remobilized.

v) A reverse engineering approach allowed to calculate the local lahar velocities (2-4 m/s, with peaks of 13-15 m/s), dynamic pressures (4-8 kPa, with peaks of 90-115 kPa), and solid volumetric concentration (~30%, implying a 1:3 ratio between deposit and flow thickness), on the basis of the external clast properties entrained into the flows then emplaced into the ash matrix, and on the presence of the lahar deposits in proximity of obstacles and archaeological findings.

As a general conclusion, we have demonstrated that the areal impact of both primary deposits and lahars, in case of sub-Plinian events at Somma-Vesuvius, involves a territory wider than previously known and for several years, with possible decreasing damages over time.

Appendix A. Calculation of lahar velocities and dynamic pressures

A theoretical scheme is presented to quantify local velocities and dynamic pressures of the lahars, by inverting the field features at selected locations. The final goal is to map the values of velocity and dynamic pressure to assessing the hazard from lahars in the study area. Flow dynamic pressure, P_{dyn}, results from a combination of flow density, ρ_f, and flow velocity, v, and is defined as follows

$$P_{dyn} = 0.5\rho_f v^2 \quad \text{(A1)}$$

In the study area, the original flow was a multiphase flow of water + pyroclastic sediment, which during remobilization evolved into a flow of water + pyroclastic sediment + external clasts. Generically, flow density results from a combination of particle density, ρ_p, and water density, ρ_w, through particle volume concentration, C, and is defined as follows

$$\rho_f = \rho_p C + \rho_w (1 - C) \quad \text{(A2)}$$

In order to define flow velocity, we take into account stratigraphic and sedimentological characteristics of the lahar flow units: i) they are ubiquitously massive, and result from remobilization of the primary pyroclastic deposits then emplacement from mass flows; ii) they contain big external clasts entrained (by dynamic pressure) and uplifted (also by pore pressure) from substrate into the flows. With these field characteristics, flow velocity can be expressed as a combination of entrained clast properties and flow density, and is defined as follows (modified after Roche, 2015)

$$v = \sqrt{\frac{X\psi\left(\rho_c - \rho_w\right)g}{\gamma\rho_f}} \qquad \text{(A3)}$$

where X is clast small axis, Ψ is clast shape factor, ρ_c is clast density, g is gravity acceleration and γ is an empirical constant. Eq. 3 allows quantifying the incipient motion of the big clasts, and gives minimum values of flow velocity required to entrain and uplift the clasts from substrate, probably more than once, before being emplaced into the lahar deposits by flow velocity drop. Such equation has been originally derived in laboratory experiments for a multiphase flow of air + sediment, and is highly performing at $\rho_f \sim 1000$ kg/m^3 (hindered settling) for dense pyroclastic currents controlled by topography then opened to alluvial plain (Martí et al., 2019), which is a case similar to the lahars in the study area. Substituting Eq. 3 into Eq. 1 and simplifying gives

$$P_{dyn} = 0.5\frac{X\psi\left(\rho_c - \rho_w\right)g}{\gamma} \qquad \text{(A4)}$$

For given clast properties, flow dynamic pressure has a unique value, while flow velocity is a function of flow density. Indeed, the present scheme is a spot model that basically depends on, and is limited to, the finding of big clasts and boulders within the lahar deposits. An approximation is that velocity and dynamic pressure are calculated for the locations where the clasts are found in the deposits, meaning that the calculated values are overestimated for those exact locations, while they are more properly referred to the immediate surroundings upstream.

At the selected locations in the study area, we collected the dimensions of the biggest clasts found in the lahar deposits, and we characterized lithologically the clasts in the field, to calculate flow dynamic pressures using Eq. 4. We used the following values for the various parameters in the calculations: Ψ

(ellipsoid) = 0.66; ρ_c (limestone) = 2500 kg/m^3; ρ_c (ceramic) = 2000 kg/m^3; ρ_c (brick) = 2000 kg/m^3; ρ_c (tephra) = 1500 kg/m^3; ρ_c (lava) = 2500 kg/m^3; ρ_c (iron) = 8000 kg/m^3; ρ_w = 1000 kg/m^3; g = 9.81 m/s^2; γ = 0.031 – 0.071. Also, we calculated flow velocities using Eq. 3, in the following range of flow density: $\rho_w \leq \rho_f \leq \rho_p$, where ρ_w = 1000 kg/m^3 and ρ_p = 2000 kg/m^3. In this way, flow density spans from two extreme cases: i) $\rho_f = \rho_w$, negligible pyroclastic sediment and external clasts, so water flow only; ii) $\rho_f = \rho_p$, negligible water and dominant pyroclastic sediment, so ash flow only. For the empirical constant in Eq. 3, we used three different values to test the sensitivity with respect to different physical states of the multiphase flow: γ (non-fluidized) = 0.031; γ (initially fluidized and slightly expanded) = 0.057; γ (initially fluidized and non-expanded) = 0.071 (see Roche et al., 2013; Fig. A1).

Regarding flow velocity, after calculation we can rewrite Eq. 3 in a simpler form (to more directly relate velocity to density) as follows

$$v = \frac{a}{\sqrt{\rho_f}} \qquad \text{(A5)}$$

where $a > 0$ depends on clast properties, and its square has dimension of pressure. On the other hand, it is not straightforward to constrain local flow velocities with unique values of flow densities, mostly because small variations of velocity correspond to large variations of density, and this is particularly valid for volcaniclastic mass flows (Carling, 2013; Jenkins et al., 2015; Roche, 2015; Martí et al., 2019; Guzman et al., 2020; Thouret et al., 2022).

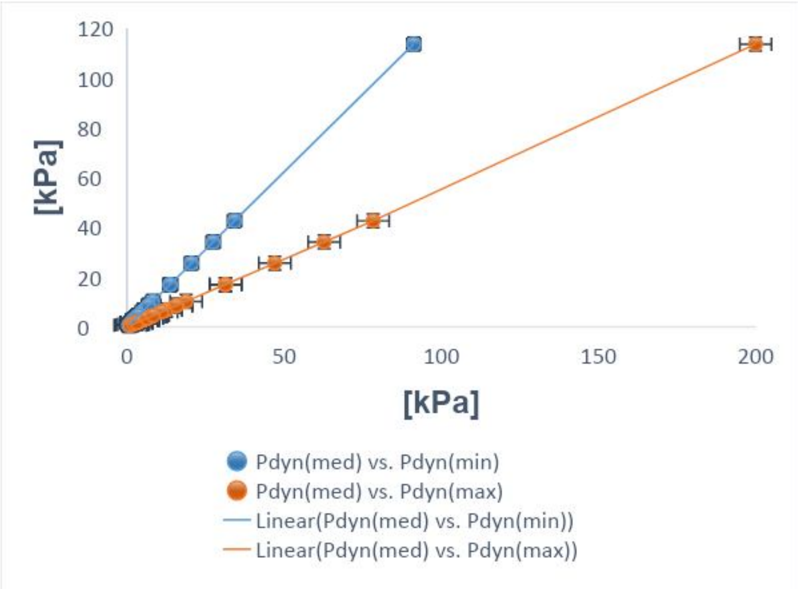
120
100
80
60
40
20
0
[kPa]
0
50
100
150
200
[kPa]
Pdyn(med) vs. Pdyn(min)
Pdyn(med) vs. Pdyn(max)
Linear(Pdyn(med) vs. Pdyn(min))
Linear(Pdyn(med) vs. Pdyn(max))

A

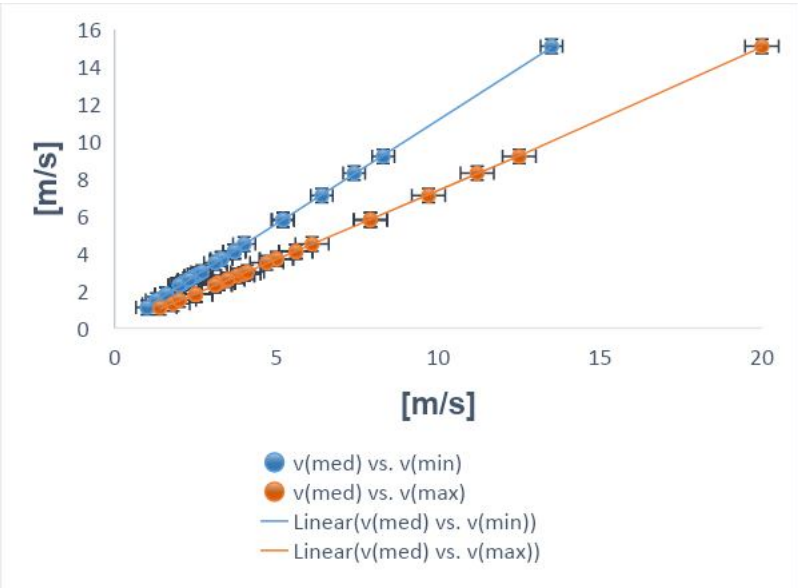
16
14
12
10
8
6
4
2
0
[m/s]
0
5
10
15
20
[m/s]
v(med) vs. v(min)
v(med) vs. v(max)
Linear(v(med) vs. v(min))
Linear(v(med) vs. v(max))

B

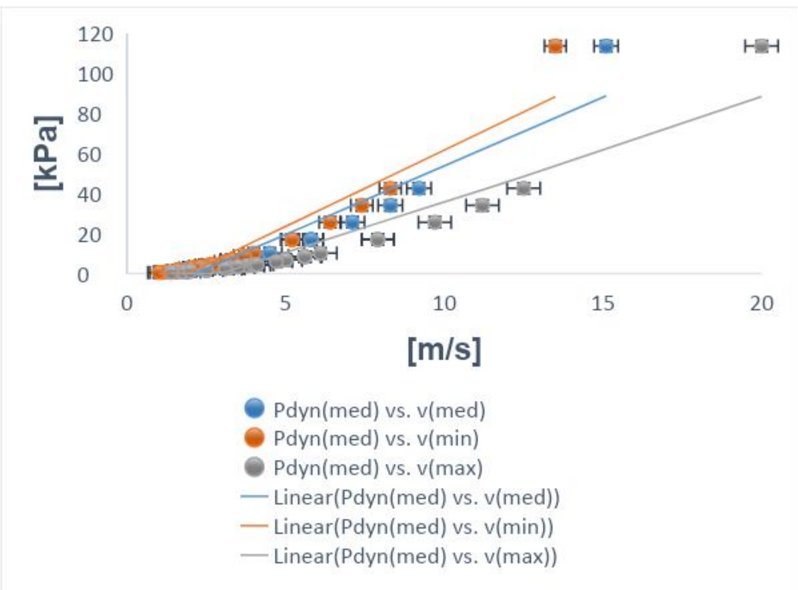
120
100
80
60
40
20
0
[kPa]
0
5
10
15
20
[m/s]
Pdyn(med) vs. v(med)
Pdyn(med) vs. v(min)
Pdyn(med) vs. v(max)
Linear(Pdyn(med) vs. v(med))
Linear(Pdyn(med) vs. v(min))
Linear(Pdyn(med) vs. v(max))

C

Fig. A1. Local dynamic pressures and velocities for the syn- and post-eruptive Pollena lahars calculated with the reverse engineering approach. **A**, dynamic pressure for the initially-fluidized and slightly expanded case vs. dynamic pressure for the initially-fluidized and non-expanded (blue) and non-fluidized (orange) cases; **B**, velocity for the initially-fluidized and slightly expanded case vs. velocity for the initially-fluidized and non-expanded (blue) and non-fluidized (orange) cases; **C**, dynamic pressure for the initially-fluidized and slightly expanded case vs. velocity for the initially-fluidized and slightly expanded (blue), vs. velocity for the initially-fluidized and non-expanded (orange), vs. velocity for the non-fluidized (grey) cases.

At some locations in the study area, we found lahar deposits against meter-scale manufacturing obstacles (Di Vito et al., 2009). The peculiarity is that the deposits in proximity of the obstacles are thicker than the correlated ones in the free field, but never reach the top of the obstacles themselves. This means that the lahars were not much expanded, so unable to overcome the obstacles as stratified flows would have done (cf. Spence et al., 2004; Gurioli et al., 2005; Doronzo, 2013; Breard et al., 2015). With this field evidence, we can assume that local flow height, H, was similar to deposit thickness against the obstacle, h_o, as follows

$$H \approx h_o \tag{A6}$$

In order to estimate flow density using Eq. 2, we focus on particle volumetric concentration. For well-sorted deposits, such concentration can be defined with an average value over flow height as follows (modified after Doronzo and Dellino, 2013; see also Eq. 30 in de' Michieli Vitturi et al., this issue)

$$C = \frac{h_f}{H} \tag{A7}$$

where h_f is deposit thickness in the free field. Substituting Eq. 6 into Eq. 7 gives

$$C \approx \frac{h_f}{h_o} \tag{A8}$$

In particular, h_f refers to those lahar deposits relatively close to the obstacles, but which were not affected by them during emplacement, i.e. close but not so much. We assessed that correlation taking into account the stratigraphic and sedimentological characteristics of the lahar deposits, and the fact that Eq. 7 performs better with layers emplaced after remobilization of primary pyroclastic fallout or dominantly ash flow deposits.

Lastly, we macroscopically assessed erosion in the field, by characterizing the unconformities present both on the primary pyroclastic and lahar deposits. In particular, the syn-eruptive lahar deposits consist of more than one flow unit, so it is important to understand how the different flow pulses interacted with each other during emplacement. The main unconformities that are found in the field are referred to the partial absence of a flow unit, and the loss of lateral continuity despite some flat geometry of the deposits. On the other hand, at some locations we were not able to assess if erosion occurred or not due to multiple open issues: i) possible absence of the primary pyroclastic deposits; ii) possible exclusive presence of the post-eruptive lahar deposits; iii) impossibility to get to some outcropping deposit base and possible unconformities.

Appendix B. Paleo-temperature and paleo-direction determinations

The magnetic fabric of a deposit was investigated by measurements of the magnetic susceptibility and its anisotropy (AMS). AMS was measured with a Kappabridge KLY-3 (AGICO), and data were elaborated by the software Anisoft5 (AGICO). AMS depends on the type, concentration, and distribution of all the minerals within the specimen. It is geometrically described by a triaxial ellipsoid, whose axes coincide with the maximum (k_1), intermediate (k_2) and minimum (k_3) susceptibility directions. The magnetic fabric of a specimen is then described by the direction of the k_1 axis, the magnetic lineation (L) and that of the k_3 axis, which is parallel to the pole of the magnetic foliation plane (F). Besides, the modulus of the susceptibility axes provides some magnetic parameters useful to express the intensity of the anisotropy (P_j) and the oblate/prolate fabric occurrence (T) (Jelinek, 1981). Generally, sedimentary vs. pyroclastic deposits fabric, here considered as the proxy of the lahar fabric, is oblate with a horizontal to gently imbricated (less than

20°) magnetic foliation. The magnetic lineation is normally clustered along the foliation plunge. In this case, both the F imbrication and the L direction can provide the local flow direction. Other times, L is orthogonal to the F plunge or F is statistically horizontal, and it is not possible to infer the flow direction.

For T_{dep} estimation, pottery sherds were subjected to progressive thermal demagnetization (PTD), with heating steps of 40 °C, up to the Curie Temperature (T_C), using the Schonstedt furnace and the spinner magnetometer JR6 (AGICO). The rationale of the method has been described in detail in several papers (McClelland and Druitt, 1989; Bardot, 2000, Porreca, 2007; Paterson et al., 2010; Lesti et al., 2011), many of them dedicated to PDCs of the Vesuvius area (Cioni et al., 2004; Di Vito et al., 2009; Giordano et al., 2018; Zanella et al., 2007; 2018; 2015). Typically, measurements are made on accidental lava lithics that were entrained during pyroclastic or lahar flows. In this case, we had the opportunity to estimate the T_{dep} by measuring ancient pottery artifacts. Briefly, pottery is characterized by a thermal remanent magnetization (TRM) acquired during its manufacture and its subsequent history of daily use. Whenever it is heated, part of its TRM, the one associated with blocking temperatures (T_b) below the heating one (T_h), is overwritten. Without alteration phenomena, the heating/cooling is a reversible process, except for the magnetic directions. The original TRM shows a random paleomagnetic direction, due to the transport during emplacement. Subsequent TRMs show directions parallel to the Earth's magnetic field during their cooling. This is clearly illustrated in the Zijderveld diagrams. The composition of the different magnetization components reveals thermal intervals characteristic of the heating history of the potsherd. Of course, this explanation is simplified, but the method is well-established and has been shown to work well with heated artifacts, such in the case of tiles and pottery embedded in the PDC deposits at Pompeii (Gurioli et al., 2005; Zanella et al.,2007), Afragola (Di Vito et al., 2009) and Santorini (Tema et al., 2015). In case of lahar, we expect low T_{dep} or cold deposits. This can be a major concern because of the difficulties to distinguish between the TRM secondary components, and the chemical (CRM) and viscous (VRM) remanent magnetization. The CRM may develop due to mineralogical changes during reheating (McClelland, 1996). Instead, VRM is typical of ferromagnetic grains with low T_b and often occurs in most rocks. Following Bardot and McClelland (2000) relationship for time intervals in the 10^2–10^6 year range, T_b=75+15 log (acquisition time in years), and using the Pollena eruption date (472 CE), e obtain a lower limit of the T_b around 123 °C. This means that this temperature helps us in discriminating between “hot” (T_b > 120 °C) or “cold” lahar (Tb < 120 °C).

Finally, routine magnetic measurements on the lahar matrix were done on the lahar matrix to determine the Characteristic Remanent Magnetization (ChRM) by Thermal and Alternating Field demagnetizations. The direction of the Earth’s Magnetic Field during the Pollena eruption is well-known (Zanella et al., 2008). If the sampled lahars were emplaced shortly after the eruption, both the secondary TRMs and the matrix of the lahars should show a remanent magnetization direction similar to the Pollena ones. ChRMs can also test if the two lahars (Acerra at 12 km from Somma-Vesuvius, and Nola at 10-15 km from Apennine source valleys) are coeval.

Appendix C. Description of the studied areas

Area 1 – Nola

In the area surrounding Nola (10-15 km from Apennine source valleys), it is possible to recognize the complete fallout sequence of the Pollena eruption (a in Fig. C1 and C2), which usually covers ploughed soils (p in Fig C1) and late Roman archaeological remains. The sequence is composed of an alternation of coarse pumice and thin ash fallout layers. Its top is always made of a fine ash bed related to the phreatomagmatic phase of the eruption (b in Fig. C1 and C2), with a thickness ranging from 1 to 14 cm due to erosion. They are almost always overlain by lahar deposits composed of several flow units (c in Fig. C1 and C2) with a large thickness variability due to channeling and presence of barriers and buildings. They sometimes include blocks, tiles, and other archaeological remains.

In Fig. C1, above the primary deposit, there is an example of a well-exposed sequence composed of at least five units (c in Fig. C1). The first one is a massive and matrix-supported deposit composed of fine and not vesiculated ash (lithofacies Gms), with fragments of greenish to blackish scoriae and minor fragments of pumices, lavas and limestones. The fragments are cm-sized and are both angular and rounded. The second flow unit is similar to the one below, but is darker and contains less coarse fragments. Its matrix is composed of an alternation of fine to medium ash layers. It follows a plane-parallel sequence of well-sorted fine sand and silt layers characterized by the lithofacies fM. A massive deposit follows upward, it is progressively humified and contains abundant reworked and rounded pumice clasts from the Avellino eruption. The top humified surface is almost always eroded by anthropogenic activity and is generally ploughed (p1 in Fig. C2). It is overlain by the primary deposits of the 1631 eruption (d in Fig. C2). It is few cm thick and is composed of a basal layer of dark coarse ash (small pumice fragments), overlain by a massive ash bed, containing abundant accretionary lapilli. The following deposit thickens in the ploughing furrows and depressions, and is composed of massive fine-ash beds, vesiculated and cohesive, and is interpreted as a lahar deposit (lithofacies mM) (e in Fig. C2). This deposit (e in Fig. C3) overlies the foundations of Palazzo Orsini (blocks in Fig. C3), now seat of the Court of Nola and built in the second half of the XV century (Fig. C3). The top is always eroded by the modern anthropogenic activity, and locally by deposits of recent eruptions of Vesuvius (e.g., 1822, 1906).

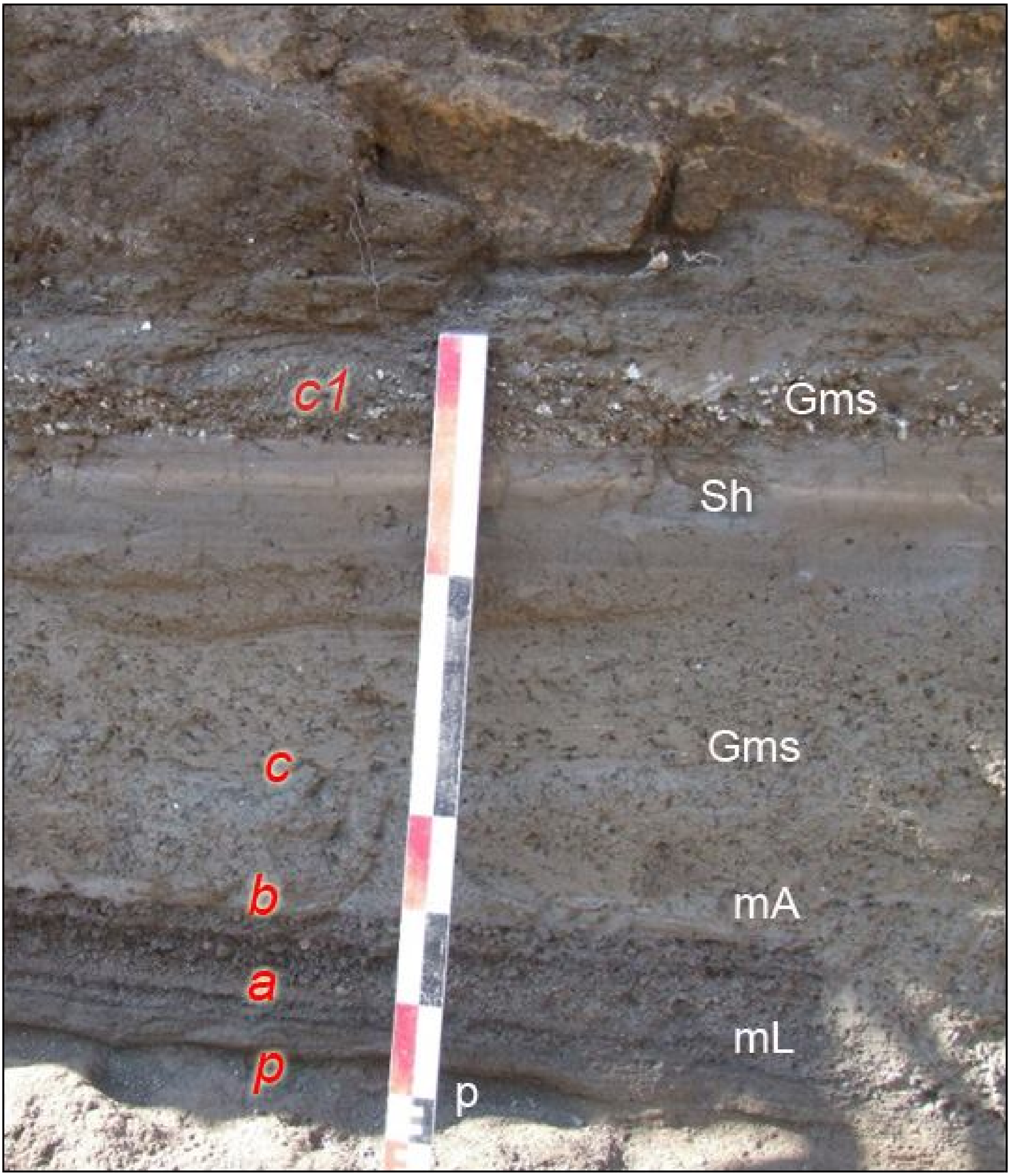

Fig. C1. Nola (10-15 km from Apennine source valleys), Pollena fallout deposits overlain by at least five lahar units. In particular: p = paleosol; a = alternation of coarse and fine fallout sequence of the Pollena eruption; b = final ash fallout of the eruption; c = sequence of syn-eruptive lahars; c1 = post-eruptive lahar containing white pumice fragments of the Pomici di Avellino eruption. For the description of lithofacies see Tab. 2.

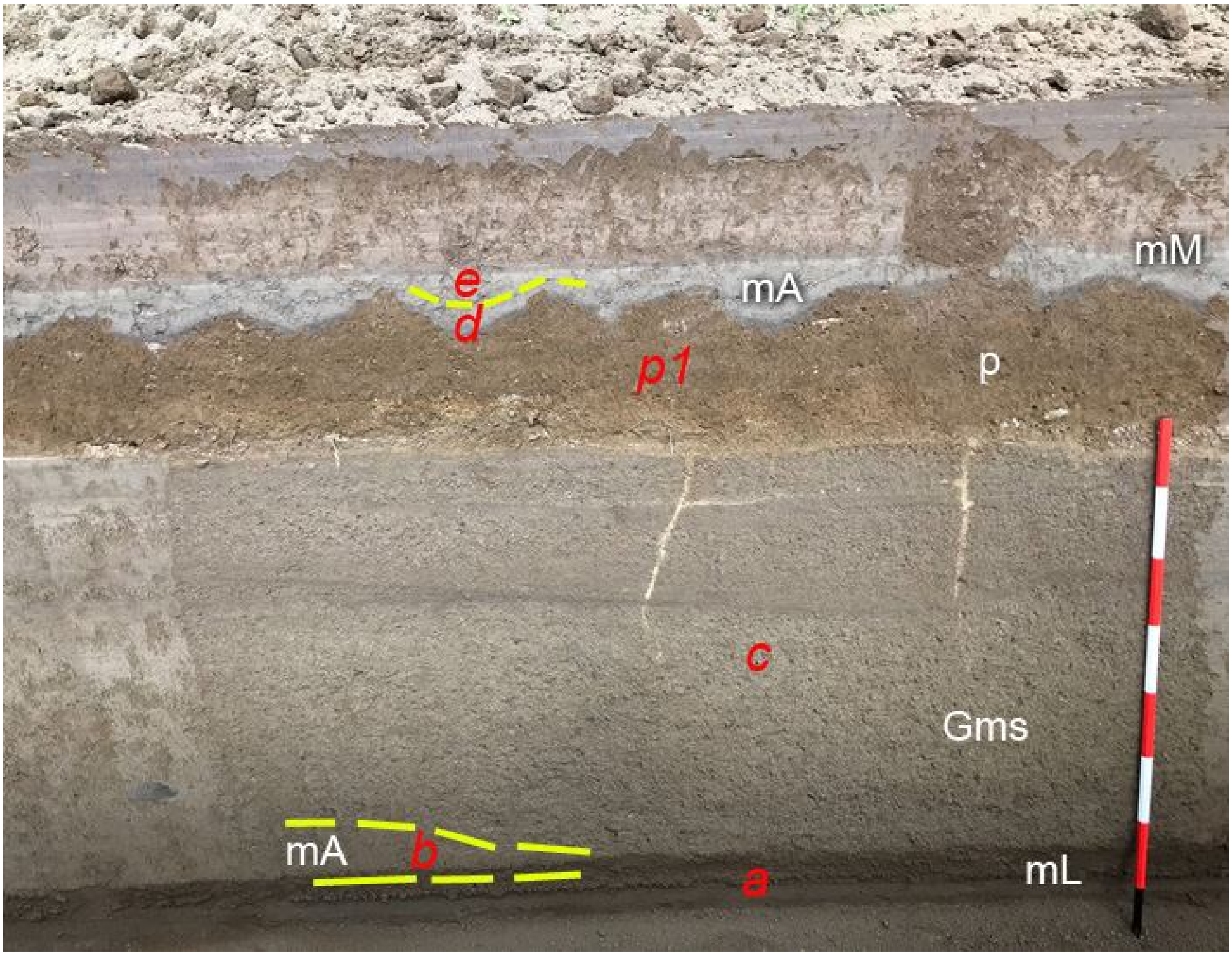

Fig. C2. Nola, Pollena lahar deposits overlain by a cultivated paleosol, and by the 1631 ash fallout and lahars. In particular: a = alternation of coarse and fine fallout sequence of the Pollena eruption; b = final ash fallout of the eruption, partially eroded; c = sequence of three lahar units; p1 = ploughed paleosol; d = 1631 ash fallout deposit mantling the undulated paleosol; e = lahar deposit composed of a massive ash layer. For the description of lithofacies see Tab. 2.

Fig. C3. Palazzo Orsini, Nola (1631 fallout and lahars). In particular: d = 1631 ash fallout deposit overlying the foundations of the building (in the inset); e = syn-eruptive lahar deposit. For the description of lithofacies see Tab. 2.

In Nola and in the nearby Cimitile (about 10-15 km from Apennine source valleys), the effects on the territory of the lahar emplacement related to the Pollena eruption are testified by numerous archaeological remains. The Nola and Cimitile areas are covered by thick sequences of fallout and lahar deposits. In fact, the previous ground level was at least 2-3 m below the present one. This effect is well visible in the Amphitheater Laterizio, which was completely filled by the primary and secondary deposits, and the same in Cimitile, where in the archaeological site of the Early Christian basilicas the present ground level is about two meters higher than the one before the eruption. It is worth noting that in Cimitile the flows were able to carry limestone blocks of 50 cm in diameter, likely along the main flow direction of the lahars (Fig. C4).

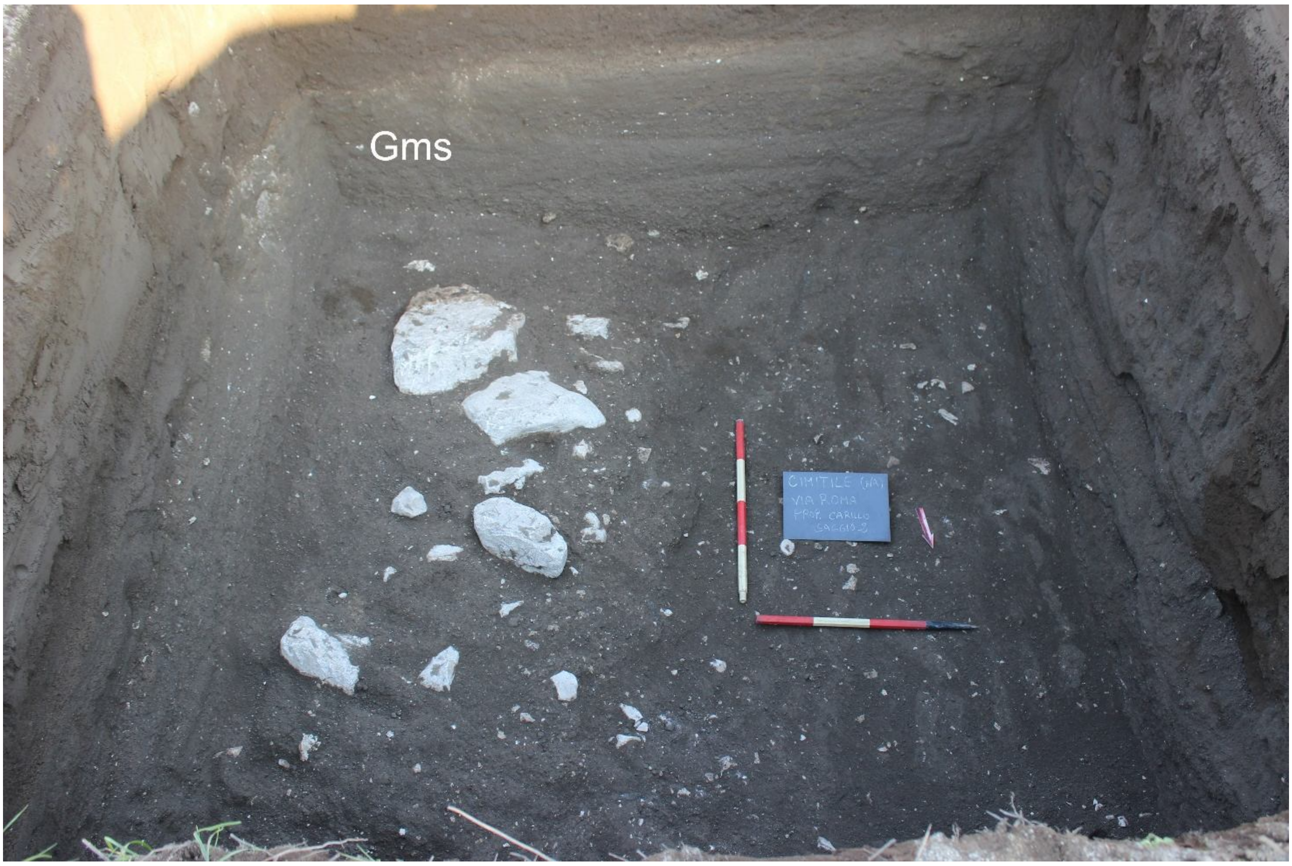

Fig. C4. Cimitile, sequence of three m-thick syn-eruptive lahar units with the evidence of transport of calcareous block (up to 50 cm). The largest are in the lower unit. The base of the lahar sequence and the underlying fallout deposit of the Pollena eruption are not visible in the photo. For the description of lithofacies see Tab. 2.

Area 2 – Acerra-Afragola

The Acerra and Afragola territories (about 12 km from Somma-Vesuvius) are located north and north-west of Vesuvius, and are almost flat areas crossed by the Clanis river. Both the coarse fallout deposits of the Pollena and 1631 eruptions are absent in this area. Here, only a thin, centimetric ash bed overlies the Late Roman paleosol. This fine ash bed, which we correlate with the final phreatomagmatic phases of the Pollena eruption, is homogeneous, cohesive and mantles the ground without any significant lateral variation. The overlying deposit is characterized by high thickness variations, it is generally massive and contains vesicles from circular to flattened and coated by fine ash. It has a matrix-supported texture and is composed of fine to very fine, very cohesive ash, and contains scattered and more or less abundant pumice and lithic fragments (lithofacies mM) and remains of vegetation (Barone et al., 2023). From one to three depositional units have been recognized, marked by unconformities, and differences in grain-size or color. The uppermost unit always contains white pumice fragments of the Avellino eruption. Very common are drying out structures and water escape structures, which are vertical structures (Fig. C5) looking like fractures a few cm large, filled by finer material transported by the escaping water, formed soon after the emplacement of the sequence of the syn-eruptive lahars (Fig. C5). The maximum thickness recorded in this area is about 90 cm.

Fig. C5. Acerra (12 km from Somma-Vesuvius), lahar deposit (unit 2) overlaying a cultivated paleosol (unit 3). The index finger indicates a water escape structure crossing the sequence of lahars. For the description of lithofacies see Tab. 2.

The top is almost always horizontal due to the erosion related to the modern anthropogenic activity, and only in a few exposures it is capped by a paleosol, with traces of human presence of the Medieval times and of the deposits of the 1631 eruption as well. The base of this latter deposit is a cm-thick fine-ash bed with an internal plane-parallel layering emplaced by fallout. It underlies a massive deposit with high thickness variations (max 20 cm) at the outcrop scale. It is composed of fine ash, cohesive and vesiculated and contains scattered small pumice fragments (lithofacies mM). The pumice fragments are vesicular, dark gray to blackish, highly porphyritic with leucite, pyroxene and feldspar crystals. The stratigraphic position and lithology confirm their attribution to the 1631 primary and secondary (lahars) deposits.

Area 3 – Pomigliano-Marigliano

This area is located along the northern outer part of the Vesuvius apron (Santacroce et al., 2003). The studied sequences start from the paleosol developed on top of the ash deposits of the AD 79 eruption. The paleosol is mature and contains pottery fragments till the II century AD. Its top is undulated with traces of ploughing spaced about 50 cm (a in Fig. C6). Representative sequences of the area include a basal ash layer with a thickness ranging from 1 to 4 cm (b in Fig. C7), thickening in the depressions, cohesive and locally vesiculated. It is here interpreted as co-ignimbritic ash emplaced by fallout during the phreatomagmatic final phases of the Pollena eruption. Upwardly, the sequence includes several lahar units from massive to slightly stratified, composed of fine and very cohesive ash, and containing scattered greenish pumice fragments (lithofacies mM) (b1 in Fig. C7). Locally this deposit, also in the case of multiple units, is cut by vertical drying cracks. The sequence is overlain by a 25-30 cm thick mature paleosol, containing cultivation traces and majolica fragments (c in Figs. C6 and C7).

The top of this paleosol is undulated and covered by the primary deposit of the 1631 eruption (d in Fig. C7). This latter is represented by a discontinuous medium-to-fine ash layer, slightly laminated for contrasting grain-size, up to 5 cm thick, with a gray to violet color, and containing dark pumice fragments and loose crystals of leucite, pyroxene and biotite (Fig. C7). Its thickness variation is due both to slight internal variations (thickening in correspondence of depressions) and erosion by the following lahars. These latter are composed of one to three flow units (d1 in Fig. C7), with a cumulative total thickness varying from 10 to 45 cm. They are composed of massive fine and very cohesive ash, and contain rare scattered dark pumice fragments similar to those of the 1631 eruption (lithofacies mM). These sequences are overlain by recent, cultivated soil. Locally, thin ash beds of the recent Vesuvius activity (like 1822, 1906) overlie the 1631 deposits.

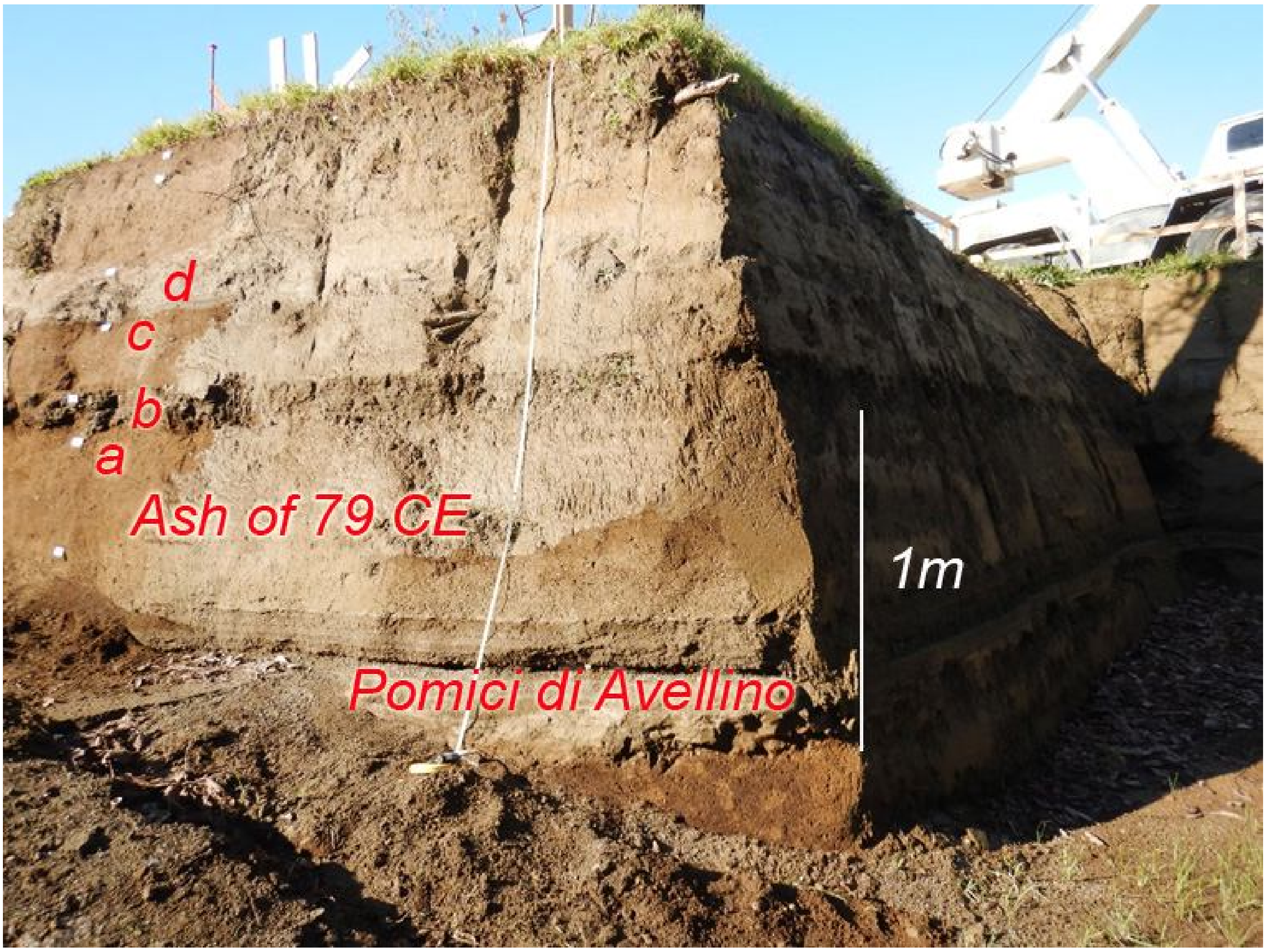

Fig. C6. Pomigliano, sequence of deposits including bottom to top: Bronze Age paleosol, Pomici di Avellino (unit EU 5 of Di Vito et al., 2009), paleosol developed on top of Pomici di Avellino and buried by the Pollena eruption deposits. In the central part, fine ash deposits of the 79 CE eruption are visible. The top of the paleosol is undulated and ploughed. In particular: a = paleosol of Roman Age; b = primary and secondary deposits of the Pollena eruption; c = paleosol between Pollena and 1631 deposits; d = 1631 primary and secondary deposits. Further details in Fig. C7.

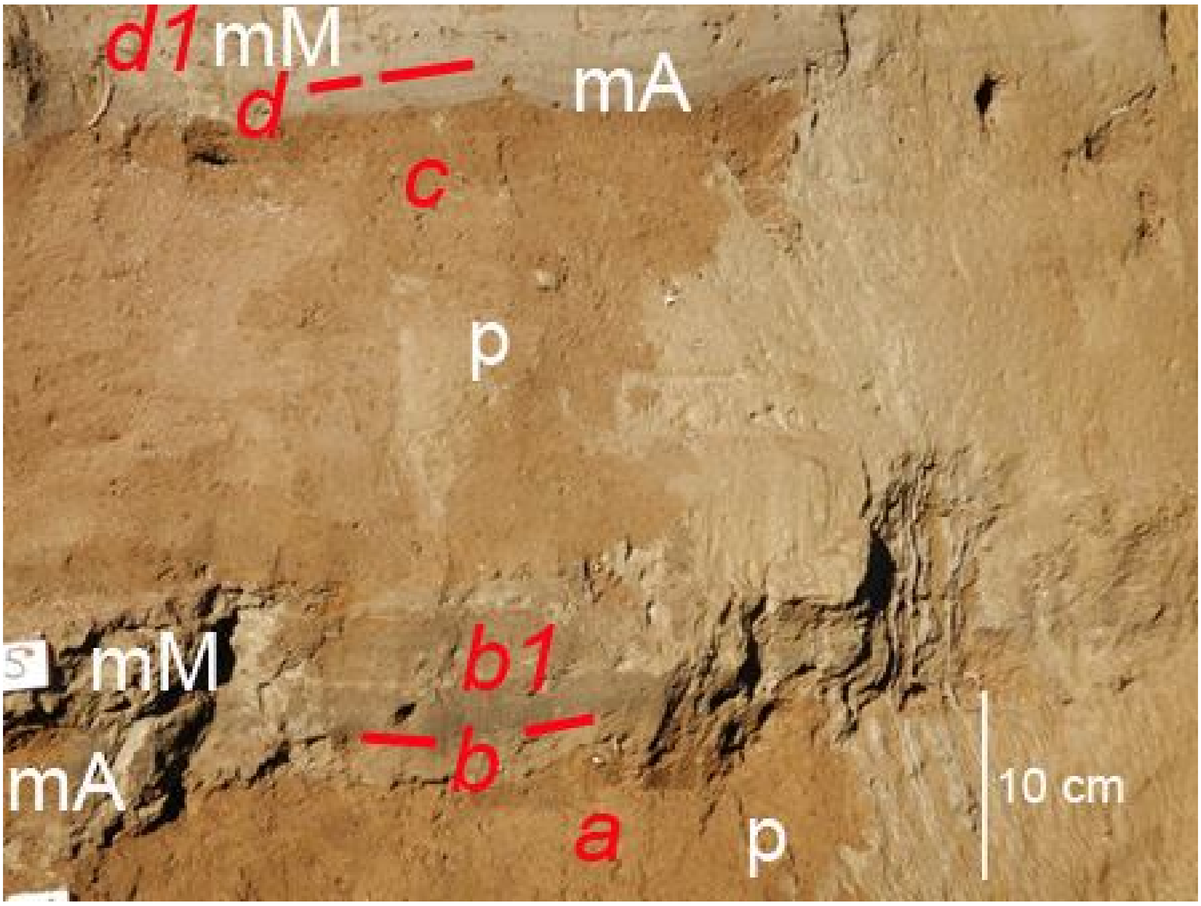

Fig. C7. Pomigliano, particular of Fig. C6: a = paleosol containing potteries of the II Cent. AD; b = ash deposit of the Pollena eruption; b1 = syn-eruptive lahars of the Pollena eruption; c = paleosol between Pollena and 1631; d = primary deposits of the 1631 eruption overlain by syn-eruptive lahars (d1). For the description of lithofacies see Tab. 2.

Area 4 – Avella-Baiano Valley

We have analyzed several sequences along the *Avella-Baiano* Valley, both exposed and excavated for the present work. Here the sequences of primary deposits are often affected by deep erosion, in fact, in some places the Pollena primary deposits are completely lacking and only the syn-eruptive lahar deposits are present on top of the late Roman paleosol. Where preserved, the paleosol has often an undulated surface due to cultivation (ploughing and hoeing). The Pollena eruption sequence consists of an alternation of coarse pumice and fine ash layers emplaced by fallout (a in Fig. C8). It is up to 50 cm thick and ends with a cohesive yellowish ash layer (b in Fig. C8), overlain by the lahar deposits, generally composed of 2-3 flow units (c in Fig. C8). The total thickness of the lahars is largely variable with maxima at the base of the slopes where it can reach 2-3 m. In some excavations we did not reach the base of the deposit, deeper than 3.5 m. In Fig. C8, it is possible to observe a complete sequence of the Pollena deposits overlying a late Roman paleosol. The sequence includes the fallout layers and thick lahar deposits. These latter are always massive, matrix-supported, and contain abundant scattered pumice and lithic fragments (lithofacies Gms). In some cases, the lower part contains several limestone fragments up to 10 cm in diameter. The described deposit has been also found in the Roman Amphitheatre of Avella, where it has a variable thickness (order of decimetric). Here, it has been almost all excavated and only remnants are presently exposed.

Generally, the upper part of the sequences is composed of an alternation of plane-parallel to cross-layered sands and gravels, with abundant rounded limestone fragments, emplaced by several alluvial episodes (post-eruptive) (lithofacies Sh-Ss). In these post-eruptive deposits, it is not uncommon to find terracotta fragments from the Imperial Roman age.

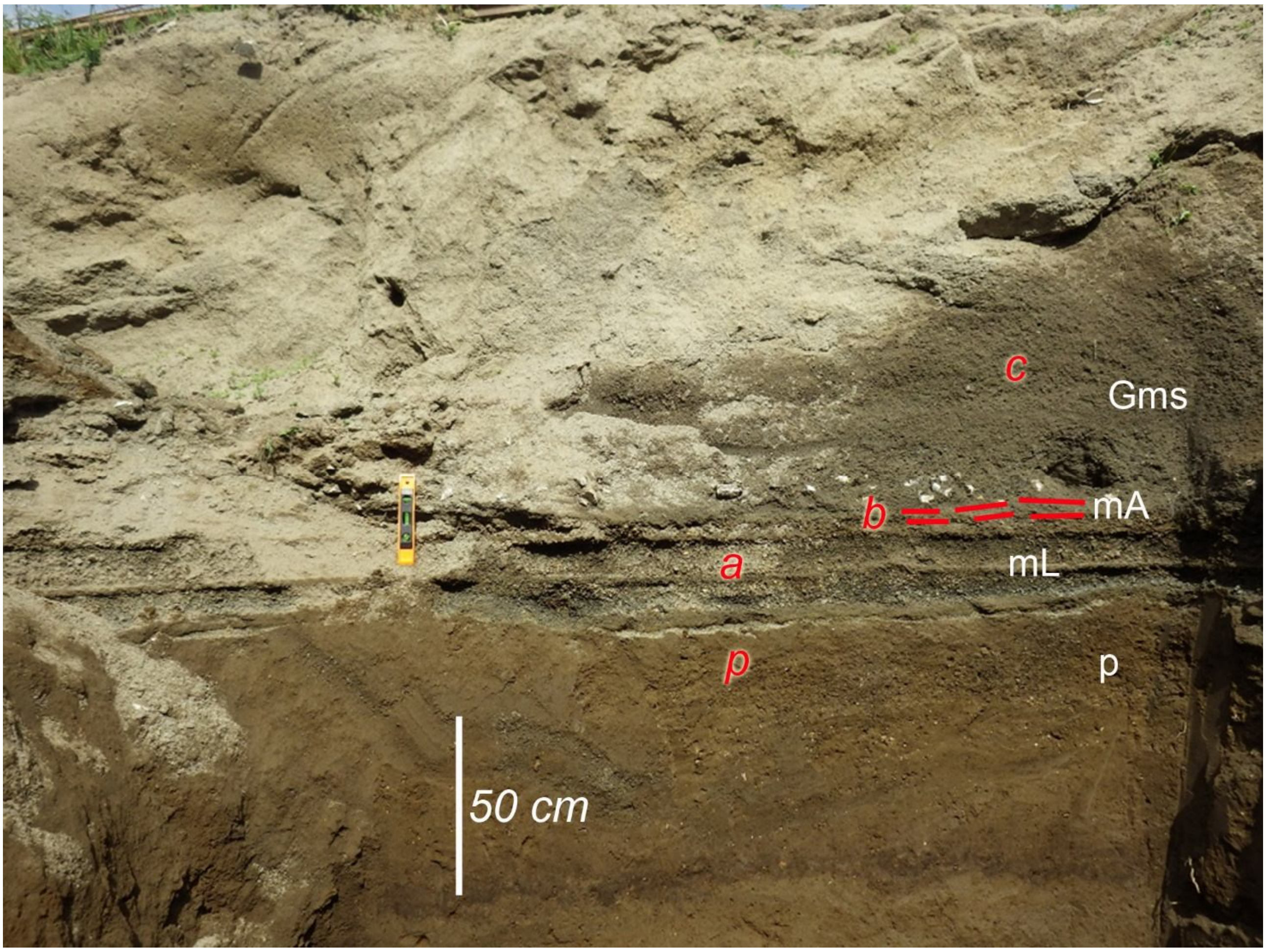

Fig. C8. Avella-Baiano Valley, the Pollena primary deposit (a,b) lies on a ploughed soil (p), and is covered by at least three flow units of lahars (c). For the description of lithofacies see Tab. 2.

The Pollena primary and secondary sequences are overlain by a mature paleosol with frequent evidence of cultivation (ploughing, p in Fig. C9) and locally by the 1631 eruption deposits. The primary deposit related to the 1631 eruption is not always present. It is up to 2 cm (a in Fig. C9) thick ash layer, gray-violet in color deposited by fallout deposit and overlaying a ploughed paleosol (p in Fig. C9). It is overlain by lahar deposits (b in Fig. C9) composed of several units and characterized by contrasting grain-sizes. The deposits are composed of medium ash, are massive and matrix-supported, and contain abundant scattered mm- to cm-sized pumice fragments (all with the same lithology of the primary deposits) and sometimes vegetal remain traces (lithofacies Gms).

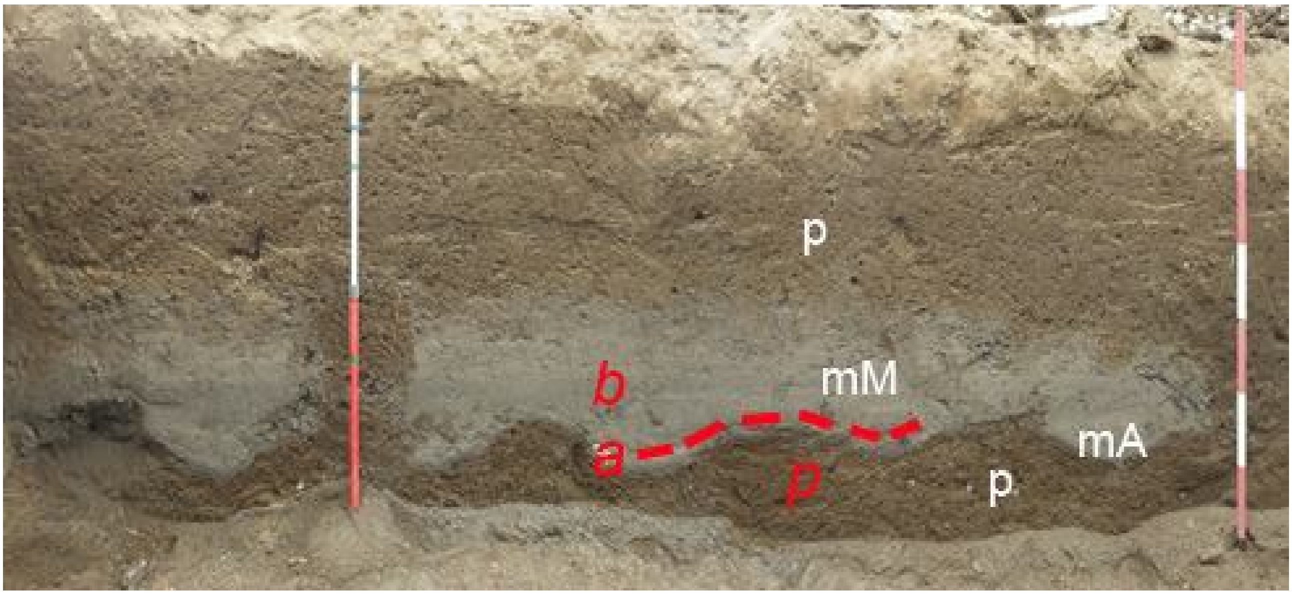

Fig. C9. Avella-Baiano Valley, particular of the 1631 primary (a) and secondary deposits (b, syn-eruptive lahars) in a trench at Cicciano locality. For the description of lithofacies see Tab. 2.

Area 5 – Lauro Valley

Lauro Valley has characteristics similar to the Avella-Baiano Valley, but the primary deposits of Pollena and 1631 eruptions are thicker (Figs. 5 and 6) and coarser. In this valley, also the sequences are locally deeply eroded. In fact, the deposits of the Pollena eruption (normally 50-70 cm thick) (Fig. C10) are sometimes missing. They overlie a mature paleosol with abundant traces of cultivation. Overall, the characteristics of the deposits are very similar to the ones of the Nola area (10-15 km from Apennine source valleys). The overlying lahar deposits are always massive, matrix-supported, and composed of fine and very cohesive ash with abundant scattered pumices and lithic fragments (similar in lithology to those of the primary deposits) (lithofacies Gms). These deposits have a high variable thickness, with a measured maximum of 2 m, but sometimes reduced by erosion. In some trenches the base of the sequences was deeper than the investigated depth (>3.5 m).

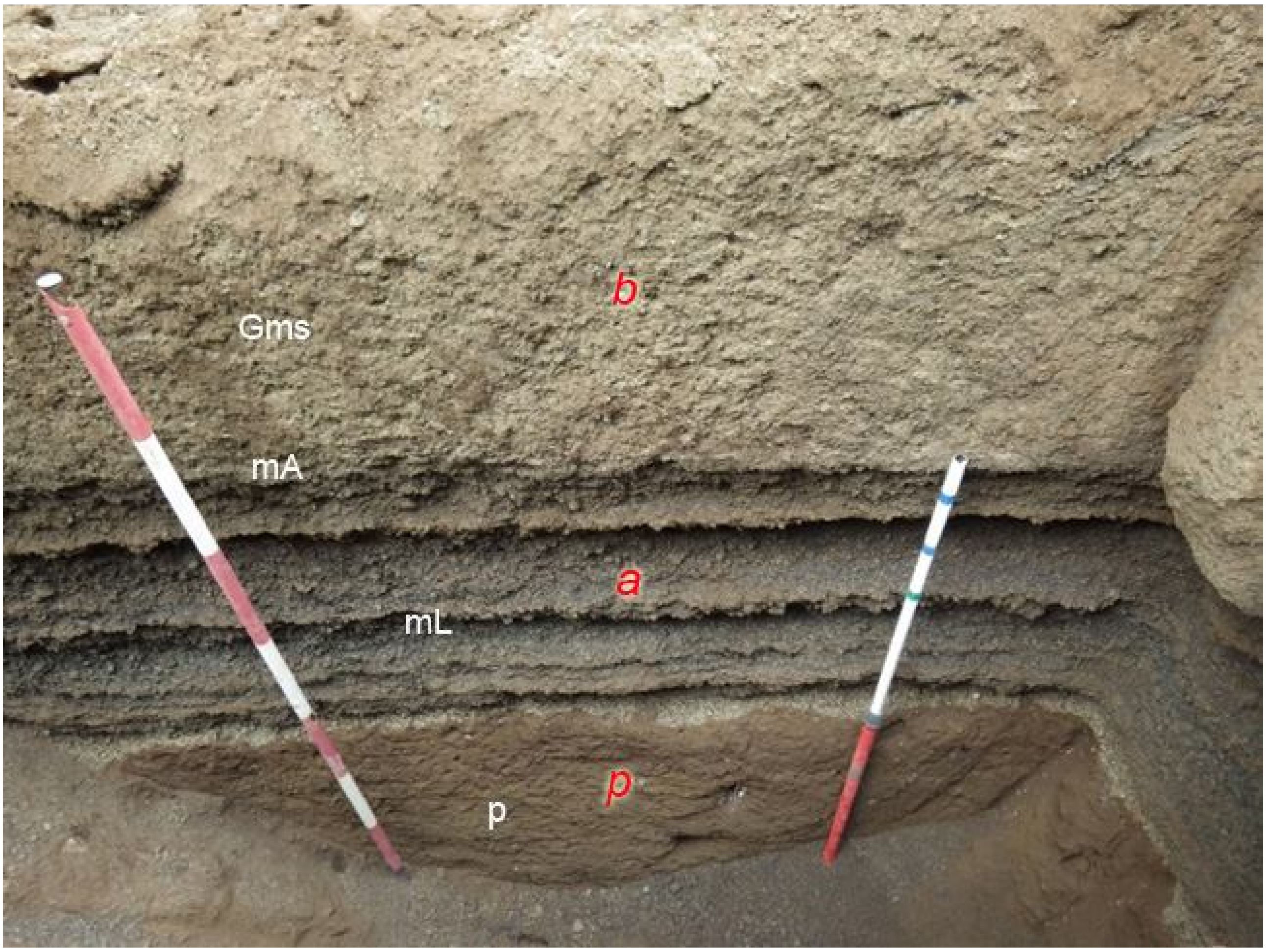

Fig. C10. Lauro Valley, Pago del Vallo, in particular: a = sequence of the Pollena fallout deposits overlain by syn-eruptive lahars (b); p = late Roman paleosol at the base. For the description of lithofacies see Tab. 2.

It is possible to evaluate the effects of the lahars on building in the Roman Villa di Lauro, at Taurano, where a 70 cm thick fallout is overlain, without paleosol, by syn-eruptive lahars which engulfed and transported pieces of walls, bricks and potteries. The lahar deposits are matrix supported and composed of fine to coarse ash and contain abundant pumice lapilli (all similar to the Pollena fallout deposits). They are massive, cohesive and have a thickness up to about 1 m, thickening in depressions and near barriers (Fig. C11).

The sequence related to the eruption of 1631 is not always present, but it is possible to find its primary deposit, composed of a basal layer of stratified fine and medium thin ash beds, and minor dark pumice and lithic fragments overlain by a thin, very fine and cohesive accretionary lapilli-rich ash bed. The maximum measured thickness is 30 cm. The overlying lahar deposits are massive and matrix-supported, composed of fine to coarse ash and contain abundant pumice fragments of the primary deposit.

Fig. C11. Taurano (Villa Lauro), baulk showing a thick sequence of the Pollena syn-eruptive lahar units filling the Roman Villa. Some units engulf and transport pieces of walls and large blocks. The fallout sequence is not exposed in the Villa, likely due to the presence of a roof. The deposit below the damaged walls is composed of multiple lahar units represented by the Gms lithofacies (see Tab. 2).

Author contribution

MDV: conceptualization, investigation, methodology, writing - original draft preparation, writing - review & editing, funding acquisition; IR: data curation, investigation, writing - original draft preparation; SdV: investigation, writing - original draft preparation, writing - review & editing; DMD: investigation, methodology, data curation, writing - original draft preparation, writing - review &

editing; MB: data curation, methodology, writing - original draft preparation; MdMV: writing - review & editing; MR: conceptualization, writing - review & editing; LS: writing - review & editing; GZ: investigation, writing - review & editing; EZ: investigation, methodology, writing - original draft preparation; AC: conceptualization, writing - review & editing, funding acquisition.

Competing interests The authors declare no competing interests

Acknowledgements

This work benefited of the agreement between Istituto Nazionale di Geofisica e Vulcanologia and the Italian Presidenza del Consiglio dei Ministri, Dipartimento della Protezione Civile (DPC), Convenzione INGV-DPC All. B2. The work was also supported by the INGV project Pianeta Dinamico—Working Earth (CUP 1466 D53J19000170001—"Fondo finalizzato al rilancio degli investimenti delle 1467 amministrazioni centrali dello Stato e allo sviluppo del Paese", legge 145/2018)—Task V3 (MDV). The Soprintendenza Archeologica, Belle Arti e Paesaggio per l'area Metropolitana di Napoli e per le Province di Salerno e Avellino is warmly acknowledged for giving access to archaeological excavations, The paper does not necessarily represent DPC official opinion and policies. We thank very much Ulrich Kueppers, Lucia Capra, an anonymous reviewer and the editor Andrea Di Muro for their help in improving this manuscript in the revision process.

References

Acocella V and Funiciello R (2006) Transverse systems along the extensional Tyrrhenian margin of Central Italy and their influence on volcanism. Tectonics 25,1-24.

Arguden AT and Rodolfo KS (1990) Sedimentologic and dynamic differences between hot and cold laharic debris flows of Mayon Volcano, Philippines. Geological Society of America Bulletin 102, 865-876.

Bardot L (2000) Emplacement temperature determinations of proximal pyroclastic deposits on Santorini, Greece, and their implications. Bulletin of Volcanology 61, 450-467.

Bardot L, McClelland E (2000) The reliability of emplacement temperature estimates using paleomagnetic methods: a case study from Santorini, Greece. Geophysical Journal International 143, 39-51.

Bartole R (1984) Tectonic Structure of the Latian-Campanian Shelf (Tyrrhenian Sea). Bollettino di Oceanologia Teorica Applicata 2, 197-230.

Baumann V, Bonadonna C, Cuomo S, Moscariello M (2020) Modelling of erosion processes associated with rainfall-triggered lahars following the 2011 Cordon Caulle eruption (Chile). Journal of Volcanology and Geothermal Research 390, 106727.

Bisson M, Pareschi MT, Zanchetta G, Sulpizio R, Santacroce R (2007) Volcaniclastic debris-flow occurrences in the Campania region (Southern Italy) and their relation to Holocene–Late Pleistocene pyroclastic fall deposits: implications for large-scale hazard mapping. Bulletin of Volcanology 70, 157-167.

Bisson M, Spinetti C, Sulpizio R (2014) Volcaniclastic flow hazard zonation in the Sub-Apennine Vesuvian area using GIS and remote sensing. Geosphere 10, 1419-1431.

Bisson M, Zanchetta G, Sulpizio R, Demi F (2013) A map for volcaniclastic debris flow hazards in Apennine areas surrounding the Vesuvius volcano (Italy). Journal of Maps 9, 230-238.

Blott SJ and Pye K (2001) Gradistat: A Grain Size Distribution and Statistics Package for the Analysis of Unconsolidated Sediments. Earth Surface Processes and Landforms 26, 1237-1248.

Braccini GC (1632) Dell'Incendio Fattosi nel Vesuvio a XVI di Dicembre MDCXXXI. Secondino Roncagliolo, 104 pp.

Brancaccio L, Cinque A, Romano P, Rosskopf C, Russo F, Santangelo N, Santo A (1991) Geomorphology and neotectonic evolution of a sector of the Tyrrhenian flank of the Southern Apennines (Region of Naples, Italy). Zeitschrift für Geomorphologie Supplement Bd. 82, 47-58.

Breard ECP, Lube G, Cronin SJ, Valentine GA (2015) Transport and deposition processes of the hydrothermal blast of the 6 August 2012 Te Maari eruption, Mt. Tongariro. Bulletin of Volcanology 77, 100.

Breard ECP, Lube G (2017) Inside pyroclastic density currents – uncovering the enigmatic flow structure and transport behaviour in large-scale experiments. Earth and Planetary Science Letters 458, 22-36.

Brocchini D, Principe C, Castradori D, Laurenzi MA, Gorla L (2001) Quaternary evolution of the southern sector of the Campanian Plain and early Somma-Vesuvius activity: insights from the Trecase 1 well. Mineralogy and Petrology 73, 67-91.

Capra L, Sulpizio R, Marquez-Ramirez VH, Coviello V, Doronzo DM, Arambula-Mendoza R, Cruz S (2018) The anatomy of a pyroclastic density current: the 10 July 2015 event at Volcan de Colima (Mexico). Bulletin of Volcanology 80, 34.

Carling PA (2013) Freshwater megaflood sedimentation: What can we learn about generic processes? Earth-Science Reviews 125, 87-113.

Carrara E, Iacobucci F, Pinna E, Rapolla A (1973) Gravity and magnetic survey of the Campanian volcanic area, S. Italy. Bollettino di Geofisica Teorica e Applicata 15, 39-51.

Cas RAF, Wright HMN, Folkes CB, Lesti C, Porreca M, Giordano G, Viramonte JG (2011) The flow dynamics of an extremely large volume pyroclastic flow, the 2.08-Ma Cerro Galán Ignimbrite, NW Argentina, and comparison with other flow types. Bulletin of Volcanology 73, 1583-1609.

Cinque A and Robustelli G (2009) Alluvial and coastal hazards caused by long-range effects of Plinian eruptions: The case of the Lattari Mts. After the AD 79 eruption of Vesuvius. Geological Society London Special Publications 322, 155-171.

Cioni R, Santacroce R, Sbrana A (1999) Pyroclastic deposits as a guide for reconstructing the multi-stage evolution of the Somma-Vesuvius Caldera. Bulletin of Volcanology 60, 207-222.

Cioni R, Gurioli L, Lanza R, Zanella, E (2004) Temperatures of A.D. 79 pyroclastic density current deposits (Vesuvius, Italy). Journal of Geophysical Research 109, B02207.

Costa JE (1997) Hydraulic modeling for lahar hazards at Cascades volcanoes. Environmental Engineering Geoscience 3, 21-30.

D’Argenio B, Pescatore TS, Scandone P (1973) Schema geologico dell’Appennino meridionale (Campania e Lucania). In: Moderne vedute sulla geologia dell’Appennino. Convegno (Roma, 16-18 Febbraio 1972). Accademia Nazionale dei Lincei, Problemi Attuali di Scienza e Cultura, Quaderni 183, 49-72.

de' Michieli Vitturi M, Costa A, Di Vito MA, Sandri L, Doronzo DM (this issue). Lahar events in the last 2,000 years from Vesuvius eruptions. Part 2: Formulation and validation of a computational model based on a shallow layer approach.

De Simone GF, Perrotta A, Scarpati C (2011) L’eruzione del 472 d.C. ed il suo impatto su alcuni siti alle falde del Vesuvio. Rivista Studi Pompeiani 22, 61.71.

De Vivo B, Rolandi G, Gans PB, Calvert A, Bohrson WA, Spera FJ, Belkin HE (2001) New constraints on the pyroclastic eruptive history of the Campanian volcanic Plain (Italy). Mineralogy and Petrology 73, 47-65.

Di Crescenzo G and Santo A (2005) Nuovo contributo sul ruolo svolto dai livelli pomicei nelle aree di distacco delle frane di colata rapida dei massicci carbonatici campani. Convegno Nazionale La mitigazione del rischio da colate di fango a Sarno e negli altri Comuni colpiti dagli eventi del maggio 1998. Napoli, 2 e 3 maggio 2005 - Sarno 4 e 5 maggio 2005.

Di Vito MA, Castaldo N, de Vita S, Bishop J, Vecchio G (2013) Human colonization and volcanic activity in the eastern Campania Plain (Italy) between the Eneolithic and Late Roman periods. Quaternary International 303, 132-141

Di Vito M.A., Calcaterra D., Petrosino P., Zanchetta G., De Vita S., Marotta E., Cesarano M. , De Simone A., Sansivero F., Rucco I. (2019) Landslides, volcanism and volcano-tectonics: the fragility of the Neapolitan territory. Geol. F. Trips Maps, Volume 11 (1.1)/2019. https://doi.org/10.3301/GFT.2019.01 - pp 1-53.

Di Vito MA, Sulpizio R., Zanchetta G (1998). I depositi ghiaiosi della valle dei torrenti Clanio e Acqualonga (Campania centro-orientale): significato stratigrafico e ricostruzione paleoambientale. Il Quaternario Italian Journal of Quaternary Sciences 11, 273-286.

Di Vito MA, Talamo P, de Vita S, Rucco I, Zanchetta G, Cesarano M (2019) Dynamics and effects of the Vesuvius Pomici di Avellino Plinian eruption and related phenomena on the Bronze Age landscape of Campania region (Southern Italy). Quaternary International 499, 231-244.

Di Vito M, Zanella E, Gurioli L, Lanza R, Sulpizio R, Bishop J, Tema E, Boenzi G, Laforgia E (2009) The Afragola settlement near Vesuvius, Italy: The destruction and abandonment of a Bronze Age village revealed by archeology, volcanology and rock-magnetism. Earth and Planetary Science Letters 277, 408-421.

Doronzo DM (2012) Two new end members of pyroclastic density currents: Forced-convection dominated and inertia-dominated. Journal of Volcanology and Geothermal Research 219-220, 87-91.

Doronzo DM, Martí J, Sulpizio R, Dellino P (2012) Aerodynamics of stratovolcanoes during multiphase processes. Journal of Geophysical Research 117, B01207.

Doronzo DM, Dellino P (2013) Hydraulics of subaqueous ash flows as deduced from their deposits: 2. Water entrainment, sedimentation, and deposition, with implications on pyroclastic density current deposit emplacement. Journal of Volcanology and Geothermal Research 258, 176-186.

Doronzo DM (2013) Aeromechanic analysis of pyroclastic density currents past a building. Bulletin of Volcanology 75, 684.

Duller RA, Mountney NP, Russell AJ, Cassidy NC (2008) Architectural analysis of a volcaniclastic jökulhlaup deposit, southern Iceland: sedimentary evidence for supercritical flow. Sedimentology 55, 939-964.

Faccenna C, Funiciello R, Bruni A, Mattei M, Sagnotti L (1994) Evolution of a transfer related basin: the Ardea basin (Latium, Central Italy). Basin Resources 5, 1-11.

Fedi M and Rapolla A (1987) The Campanian Volcanic Area: analysis of the magnetic and gravimetric anomalies. Bollettino della Società Geologica Italiana 106, 793-805.

Finetti I and Morelli C (1974) Esplorazione di sismica a riflessione nei Golfi di Napoli e Pozzuoli. Bollettino di Geofisica Teorica e Applicata 16, 62-63.

Fiorillo F and Wilson RC (2004) Rainfall induced debris flows in pyroclastic deposits, Campania (southern Italy). Engineering Geology 75, 263-289.

Giordano G, Zanella E, Trolese M, Baffioni C, Vona A, Caricchi C, De Benedetti AA, Corrado S, Romano C, Sulpizio R, Geshi N (2018) Thermal interactions of the AD79 Vesuvius pyroclastic density currents and their deposits at Villa dei Papiri (Herculaneum archaeological site, Italy). Earth and Planetary Science Letters 490, 180-192.

Girolami L, Roche O, Druitt T, Corpetti T (2010) Velocity fields and depositional processes in laboratory ash flows, with implications for the dynamics of dense pyroclastic flows. Bulletin of Volcanology 72, 747-759.

Gurioli L, Pareschi MT, Zanella E, Lanza R, Deluca E, Bisson M (2005) Interaction of pyroclastic density currents with human settlements: Evidence from ancient Pompeii. Geology 33, 441-444.

Gurioli L, Sulpizio R, Cioni R, Sbrana A, Santacroce R, Luperini W, Andronico D (2010) Pyroclastic flow hazard assessment at Somma-Vesuvius based on the geological record. Bulletin of Volcanology 72, 1021-1038.

Guzman S, Doronzo DM, Martí J, Seggiaro R (2020). Characteristics and emplacement mechanisms of the Coranzulí ignimbrites (Central Andes). Sedimentary Geology 405, 105699.

Ippolito F, Ortolani F, Russo M (1973) Struttura marginale tirrenica dell’Appennino campano: reinterpretazioni di dati di antiche ricerche di idrocarburi. Memorie della Società Geologica Italiana 12, 227–250.

Iverson RM, Denlinger RP, LaHusen RG, Logan M, (2000) Two-phase debris-flow across 3-D terrain: Model predictions, *in* Wieczorek GF and Naeser ND, eds., Debris-Flow Hazard Mitigation, Mechanics, Prediction, and Assessment: Taipei, Taiwan, 16-18 August 2000: Rotterdam, Balkema, 521-529.

Jenkins SF, Phillips JC, Price R, Feloy K, Baxter PJ, Sri Hadmoko D, de Bélizal E (2015) Developing building-damage scales for lahars: application to Merapi volcano Indonesia. Bulletin of Volcanology 77, 1-17.

Lesti C, Porreca M, Giordano G, Mattei M, Cas R, Wright H, Viramonte J (2011) High temperature emplacement of the Cerro Galán and Toconquis Group ignimbrites (Puna plateau, NW Argentina) determined by TRM analyses. Bulletin of Volcanology 73, 1535-1565.

Lowe DR, Williams SN, Leigh H, Connort CB, Gemmell JB, Stoiber RE (1986) Lahars initiated by the 13 November 1985 eruption of Nevado del Ruiz, Colombia. Nature 324, 51-53.

Lowe DR (1988) Suspended-load fallout rate as an independent variable in the analysis of current structures. Sedimentology 35, 765–776.

Lube G, Cronin S, Manville V, Procter J, Cole S, Freundt A (2012) Energy growth in laharic mass flows. Geology 40, 475-478.

Macedonio G and Pareschi MT (1992) Numerical simulation of some lahars from Mount St. Helens. Journal of Volcanology and Geothermal Research 54, 65-80.

Manville V, Nemeth K, Kano K (2009) Source to sink: A review of three decades of progress in the understanding of volcaniclastic processes, deposits, and hazards. Sedimentary Geology 220, 136-161.

Mariani M and Prato R (1988) I bacini neogenici costieri del margine tirrenico: approccio sismico-stratigrafico. Memorie della Società Geologica Italiana 41, 519-531.

Marotta E., Berrino G., de Vita S., Di Vito M.A., Camacho A.G., 2022. Structural setting of the Ischia resurgent caldera (Southern Tyrrhenian Sea, Italy) by integrated 3D gravity inversion and geological models. In: Marotta, E., D'Auria, L., Zaniboni, F. and Nave, R. (eds) Volcanic Island: from Hazard Assessment to Risk Mitigation. Geological Society, London, Special Publications, 519.

Martí J, Doronzo DM, Pedrazzi D, Colombo F (2019) Topographical controls on small-volume pyroclastic flows. Sedimentology 66, 2297-2317.

McClelland E, Druitt TH (1989) Paleomagnetic estimates of emplacement temperatures of pyroclastic deposits on Santorini, Greece. Bulletin of Volcanology 51, 16-27.

McClelland E (1996) Theory of CRM acquired by grain growth, and its implications for TRM discrimination and paleointensity determination in igneous rocks. Geophysical Journal International 126, 271-280.

Newhall CG and Punongbayan R (Eds.) (1996) Fire and mud: eruptions and lahars of Mount Pinatubo, Philippines. Quezon City: Philippine Institute of Volcanology and Seismology, 1126 pp.

Orsi G, de Vita S, Di Vito MA (1996) The restless, resurgent Campi Flegrei Nested Caldera Italy.: constraints on its evolution and configuration. Journal of Volcanology and Geothermal Research 74, 179-214.

Pareschi MT, Favalli M, Giannini F, Sulpizio R, Zanchetta G, Santacroce R (2000) May 5, 1998, Debris flows in circumvesuvian areas (Southern Italy), insights for hazard assessment. Geology 28, 639-642.

Pareschi MT, Santacroce R, Sulpizio R, Zanchetta G (2002) The volcaniclastic mass flow hazard related to the remobilization of fallout deposits in southern Campania, Italy. Explosive volcanism in subduction zones, Mount Pelée, Martinique, 12-16 May 2002, abstract volume.

Patacca E and Scandone P (2007) Geology of the Southern Apennines. Bollettino della Società Geologica Italiana Special Issue 7, 75-119.

Paterson, GA, Muxwhorty AR, Roberts AP, MacNiocaill C (2010). Paleomagnetic determination of emplacement temperatures of pyroclastic deposits: un under-utilized tool. Bulletin of Volcanology, 72, 309-330.

Peccerillo A (2003) Plio-Quaternary magmatism in Italy. Episodes 26, 222-226.

Perrotta A, Scarpati C, Luongo G, Aoyagi M (2006) Burial of Emperor Augustus' villa at Somma Vesuviana (Italy) by post-79 AD Vesuvius eruptions and reworked (lahars and stream flow) deposits. Journal of Volcanology and Geothermal Research 158, 445-466.

Pierson TC (1985) Initiation and flow behavior of the 1980 Pine Creek and Muddy River lahars, Mt. St. Helens, Washington. Geological Society of America Bulletin 96, 1056-1069.

Piochi M, Pappalardo L, De Astis G (2004) Geo-chemical and isotopical variations within the Campanian Comagmatic Province: implications on magma source composition, Annals of Geophysics 47, 1485-1499.

Pittari A, Cas RAF, Monaghan JJ, Martí J (2007) Instantaneous dynamic pressure effects on the behaviour of lithic boulders in pyroclastic flows: the Abrigo Ignimbrite, Tenerife, Canary Island. Bulletin of Volcanology 69, 265-279.

Porreca M, Mattei M, Mac Niocaill C, Giordano G, McClelland E, Funiciello R (2007) Paleomagnetic evidence for low-temperature emplacement of the phreatomagmatic Peperino Albano ignimbrite (Colli Albani volcano, Central Italy). Bulletin of Volcanology 70, 877-893.

Roche O (2012) Depositional processes and gas pore pressure in pyroclastic flows: an experimental perspective. Bulletin of Volcanology 74, 1807-1820.

Roche O, Niño Y, Mangeney A, Brand B, Pollock N, Valentine GA (2013) Dynamic pore-pressure variations induce substrate erosion by pyroclastic flows. Geology 41, 1107-1110.

Roche O (2015) Nature and velocity of pyroclastic density currents inferred from models of entrainment of substrate lithic clasts. Earth and Planetary Science Letters 418, 115-125.

Rodolfo KS (2000) The hazard from lahars and jökulhlaups. In: Encyclopedia of Volcanoes: Academic Press, Philadelphia, 973-995.

Rodolfo KS and Arguden AT (1991) Rain-lahar generation and sediment-delivery systems at Mayon Volcano, Philippines: Sedimentation in Volcanic Settings, SEPM Special Publication 45, 71-87.

Rodríguez-Sedano LA, Sarocchi D, Caballero L, Borselli L, Ortiz-Rodríguez AJ, Cerca-Ruiz MF, Moreno-Chávez G, Franco Ramos O (2022) Post-eruptive lahars related to the 1913 eruption in La Lumbre Ravine, Volcán de Colima, Mexico: The influence of ravine morphometry on flow dynamics. Journal of Volcanology and Geothermal Research 421, 107423.

Rolandi G, Barrella AM, Borrelli A (1993) The 1631 eruption of Vesuvius. Journal of Volcanology and Geothermal Research 58, 183-201.

Rolandi G, Munno R, Postiglione I (2004) The A.D. 472 eruption of the Somma volcano. Journal of Volcanology and Geothermal Research 129, 291-319.

Rosi M, Principe C, Vecci R (1993) The 1631 Vesuvius eruption. A reconstruction based on historical and stratigraphical data. Journal of Volcanology and Geothermal Research 58, 151-182.

Rosi M and Santacroce R (1983) The A.D. 472 “Pollena” eruption: volcanological and petrological data for this poorly-known, Plinian-type event at Vesuvius. Journal of Volcanology and Geothermal Research 17, 249-271.

Russell AJ, Knudsen O (1999) An ice-contact rhythmite (turbidite) succession deposited during the November 1996 catastrophic outburst flood (jökulhlaup), Skeidarárjökull, Iceland. Sedimentary Geology 127, 1-10.

Sandri L, de' Michieli Vitturi M, Costa A, Di Vito MA, Rucco I, Doronzo DM, Bisson M, Gianardi R, de Vita S, Sulpizio R (this issue) Lahar events in the last 2,000 years from Vesuvius eruptions. Part 3: Hazard assessment over the Campanian Plain.

Santacroce R, Cioni R, Marianelli P, Sbrana A, Sulpizio R, Zanchetta G, Donahue DJ, Joron JL (2008) Age and whole rock-glass compositions of proximal pyroclastics from the major explosive eruptions of Somma-Vesuvius: A review as a tool for distal tephrostratigraphy. Journal of Volcanology and Geothermal Research 177, 1-18.

Santacroce R., Sbrana A., Andronico D., Cioni R., Di Vito M., Marianelli P., Sulpizio R., Zanchetta G., Arrighi S., Benvenuti E., Gurioli L., Leoni F.M., Luperini W., 2003. Carta Geologica del Vesuvio in scala 1:15.000, Santacroce R., Sbrana A., eds. Cartografia derivata dai rilievi geologici in scala 1:10.000 Regione Campania e dai rilievi in scala 1:25.000 del Progetto CARG., S.EL.C.A., Firenze.

Santangelo N, Romano P, Ascione A, Russo Ermolli E (2017) Quaternary evolution of the Southern Apennines coastal plains: A review. Geologica Carpathica 68, 43-56.

Scott KM (1989) Magnitude and frequency of lahars and lahar-runout flows in the Toutle-Cowlitz River System. U. S. Geological Survey Professional Paper 1447-B, 1–33.

Scott KM, Vallance JW, Pringle PT (1995) Sedimentology, behavior, and hazard of debris flows at Mount Rainer, Washington. U. S. Geological Survey Professional Paper 1547, 1-56.

Scott KM, Macìas JL, Naranjo JA, Rodriguez S, McGeehin JP (2001) Catastrophic debris flows transformed from landslide in volcanic terrains: mobility, hazard assessment and mitigation strategies. US Geol Surv Prof Pap. 1630, 1-59.

Sheridan MF, Bonnard C, Carrero C, Siebe C, Strauch W, Navarro M, Calero JC, Trujillo NB (1999) Report of the 30 October 1998 rock fall/avalanche and breakout flow of Casita Volcano, Nicaragua, triggered by Hurracane Mitch. Landslide News 12, 2-4.

Siebe C, Schaaf P, Urrutia-Fucugauchi J (1999) Mammoth bones embedded in a late Pleistocene lahar from Popocatépetl volcano, near Tocuila, central Mexico. Geological Society of America Bulletin 111, 1550-1567.

Smith G, Williams R, Rowley PJ, Parsons DR (2018) Investigation of variable aeration of monodisperse mixtures: implications for pyroclastic density currents. Bulletin of Volcanology 80, 67.

Spence RJS, Zuccaro G, Petrazzuoli S, Baxter PJ (2004) Resistance of buildings to pyroclastic flows: analytical and experimental studies and their application to Vesuvius. Natural Hazards Review 5, 48-59.

Stanzione M, Di Vito MA, Aurino P, Lumaga MRB (2023) Sacred plant impressions from Somma-Vesuvius volcanic ash deposits: A medicinal garden in Late Antique Acerra (Naples, Campania, Italy)? Journal of Archaeological Science: Reports 47, 103802.

Sulpizio R, Mele D, Dellino P, La Volpe L (2005) A complex, Subplinian-type eruption from low-viscosity, phonolitic to tephri-phonolitic magma: the AD 472 (Pollena) eruption of Somma-Vesuvius, Italy. Bulletin of Volcanology 67, 743-767.

Sulpizio R, Zanchetta G, Demi F, Di Vito MA, Pareschi MT, Santacroce R (2006) The Holocene syneruptive volcaniclastic debris flows in the Vesuvian area: Geological data as a guide for hazard assessment. Geological Society of America Special Paper 402, 203-221.

Sulpizio R, Dellino P, Doronzo DM, Sarocchi D (2014) Pyroclastic density currents: state of the art and perspectives. Journal of Volcanology and Geothermal Research 283, 36-65.

Tema E, Zanella E, Pavón-Carrasco FJ, Kondopoulo D, Pavlides S (2015) Palaeomagnetic analysis on pottery as indicator for the pyroclastic flows deposit temperature: New data and statistical interpretation from the Minoan eruption of Santorini, Greece. Geophysical International Journal 203, 33-47.

Thouret JC, Arapa E, Charbonnier S, Guerrero A, Kelfoun K, Cordoba G, Rodriguez D, Santoni O (2022) Modeling tephra fall and sediment-water flows to assess their impact on a vulnerable building stock in the City of Arequipa, Peru. Frontiers in Earth Science 10, 865989.

Toyos G, Gunasekera R, Zanchetta G, Oppenheimer C, Sulpizio R, Favalli M, Pareschi MT (2008) GIS-assisted modelling for debris flow hazard assessment based on the events of May 1998 in the area of Sarno, Southern Italy: II. Velocity and dynamic pressure. Earth Surface Processes and Landforms 33, 1693-1708.

Vallance JW and Iverson R (2015) Lahars and their deposits. In: Sigurdsson, H., Houghton, B.F., McNutt, S.R., Rymer, H., Stix, J. (Eds.), Encyclopedia of Volcanoes. Academic Press, London, 649-664.

Vallance JW and Scott KM (1997) The Osceola mudflow from Mount Rainer: Sedimentology and hazards implications of a huge clay-rich debris flow. Geological Society of America Bulletin 109, 143-163.

Vitale S and Ciarcia S (2018) Tectono-stratigraphic setting of the Campania region (southern Italy), Journal of Maps 14, 9-21.

Voight B (1990) The 1985 Nevado del Ruiz volcano catastrophe: anatomy and retrospection. Journal of Volcanology and Geothermal Research 42, 151-188.

Waitt RB Jr, TC Pierson TC, MacLeod NS, Janda RJ, Voight B, Holcomb RT (1983) Eruption-triggered avalanche, flood, and lahar at Mount St. Helens - Effects of winter snowpack. Science 221, 1394-1397.

Walsh B, Coviello V, Capra L, Procter J, Marquez-Ramirez V (2020) Insights into the internal dynamics of natural lahars from analysis of 3-component broadband seismic signals at Volcan de Colima, Mexico.

Whipple KX, Hancock GS, Anderson RS (2000) River incision into bedrock: Mechanics and relative efficacy of plucking, abrasion, and cavitation. Geological Society of America Bulletin 112, 490-503.

White S, García-Ruiz JM, Martí-Bono C, Valero B, Errea MP, Gómez-Villar A (1997) The 1996 Biescas campsite disaster in the Central Spanish Pyrenees and its spatial and temporal context. Hydrological Processes 11, 1797-1812.

Zanchetta G, Sulpizio R, Pareschi MT, Leoni FM, Santacroce R (2004a) Characteristics of May 5-6, 1998 volcaniclastic debris flows in the Sarno area (Campania, southern Italy): relationships to structural damage and hazard zonation. Journal of Volcanology and Geothermal Research 133, 377-393.

Zanchetta G, Sulpizio R, Di Vito MA (2004b). The role of volcanic activity and climate in alluvial fan growth at volcanic areas: an example from southern Campania (Italy). Sedimentary Geology 168, 249-280.

Zanella E, Gurioli L, Pareschi MT, Lanza R (2007). Influences of urban fabric on pyroclastic density currents at Pompeii (Italy): 2. Temperature of the deposits and hazard implications. Journal of Geophysical Research 112, B05214.

Zanella E, Gurioli L, Lanza R, Sulpizio R, Bontempi M (2008). Deposition temperature of the AD 472 Pollena pyroclastic density current deposits, Somma-Vesuvius, Italy. Bulletin of Volcanology 70, 1237-1248.

Zanella E, Sulpizio R, Gurioli L, Lanza R (2015). Temperatures of the pyroclastic density currents deposits emplaced in the last 22 kyr at Somma-Vesuvius (Italy). Geological Society, London, Special Publication, The Use of Palaeomagnetism and Rock Magnetism to Understand Volcanic Processes 396.

Zaragoza G, Caballero-Garcia L, Capra L, Nieto-Torres A (2020) Lahares secundarios en el volcan Popocatepetl: El lahar Nexpayantla del 4 de febrero, 2010. Revista Mexicana de Ciencias Geologicas 37, 121-134.

Zuccaro G, De Gregorio D (2013) Time and space dependency in impact damage evaluation of a sub-Plinian eruption at Mount Vesuvius. Natural Hazards 68, 1399-1423.